Title
Transient evaluation of a soil-borehole thermal energy storage system

Authors
Başer, Tuğçe
McCartney, John S

Publication Date
2020-03-01

DOI
10.1016/j.renene.2018.11.012

Elsevier Editorial System(tm) for Renewable Energy
Manuscript Draft

Manuscript Number: RENE-D-18-02585R1

Title: TRANSIENT EVALUATION OF A SOIL-BOREHOLE THERMAL ENERGY STORAGE SYSTEM

Article Type: SI:Shallow Geothermal Energy

Keywords: Shallow geothermal energy; heat storage; unsaturated soil; solar thermal energy

Corresponding Author: Professor John S McCartney, PhD

Corresponding Author's Institution: University of California San Diego

First Author: Tugce Baser, PhD

Order of Authors: Tugce Baser, PhD; John S McCartney, PhD

Manuscript Region of Origin: USA

Highlights

- The ground temperatures in a field-scale soil-borehole thermal energy storage system were simulated under the boundary conditions associated with heat collection from solar thermal panels.
- A numerical model for coupled heat transfer and water flow considering enhanced vapor diffusion and phase change was calibrated using reconstituted specimens and validated against the measured field temperature data for heating and ambient cooling periods.
- The transient temperature measurements and simulation results indicate the positive aspects of installing thermal energy storage systems in unsaturated soils in the vadose zone.
- The simulation results indicate that a permanent decrease in the degree of saturation near the heat exchangers may have occurred. However, the zone of influence was not significant enough to have an overlapping effect between the heat exchangers for the conditions considered in this study.
- The decrease in degree of saturation led to a decrease in thermal conductivity and volumetric heat capacity near the heat exchangers that may lead to different transient responses upon subsequent heat injection events.

TRANSIENT EVALUATION OF A SOIL-BOREHOLE THERMAL ENERGY STORAGE SYSTEM

by Tuğçe Başer, Ph.D.[1] and John S. McCartney, Ph.D., P.E.[2]

ABSTRACT: This study focuses on the simulation of transient ground temperatures in a field-scale soil-borehole thermal energy storage (SBTES) system in San Diego, California. The SBTES system consists of an array of thirteen 15 m-deep borehole heat exchangers installed in conglomerate bedrock at a spacing of approximately 1.5 m. Heat collected from solar thermal panels was injected into the SBTES system over a 4-month period, after which the subsurface was monitored during a 5-month ambient cooling period. The SBTES system is located in the vadose zone above the water table with relatively dry subsurface conditions, so a coupled heat transfer and water flow model was used to simulate the ground response using thermo-hydraulic constitutive relationships and parameters governing vapor diffusion and water phase change calibrated using soil collected from the site. The simulated ground temperatures from the model match well with measurements from thermistors installed at different radial locations and depths in the SBTES system and are greater than those simulated using a conduction-only model for saturated conditions. Significant overlap between the effects of the borehole heat exchangers was observed in terms of the ground temperature. Although the numerical simulations indicate that permanent decreases in degree of saturation and thermal conductivity occurred at the borehole heat exchanger locations, the zone of influence of these changes was relatively small for the particular site conditions.

KEYWORDS: Thermal energy storage; Field-scale testing; Vertical boreholes; Unsaturated soil

[1] Assistant Professor, University of Illinois at Urbana-Champaign, Department of Civil and Environmental Engineering, 205 N. Mathews, Urbana, IL 61801; e-mail: tbaser@illinois.edu.

[2] Professor and Department Chair, University of California San Diego, Dept. of Structural Engineering. 9500 Gilman Dr., La Jolla, CA 92093-0085, mccartney@ucsd.edu.

1. INTRODUCTION

Soil-borehole thermal energy storage (SBTES) systems are used for storing heat collected from renewable sources in the subsurface so that it can be used later for space or water heating. Heat sources such as solar thermal panels generate heat during the day with a greater energy generation during summer months, so SBTES systems permit storage of the abundant and free thermal resource (Sibbitt et al. 2012, McCartney et al. 2013). SBTES systems function similarly to geothermal heat exchange systems, where a carrier fluid is circulated through a closed-loop pipe network installed in vertical boreholes backfilled with sand-bentonite. Different from boreholes in conventional geothermal heat exchange systems, the boreholes in SBTES systems are spaced relatively close together (1-2 m) in an array to concentrate heat in the subsurface (Claesson and Hellström 1981). SBTES systems are a convenient alternative to other energy storage systems as they are relatively inexpensive, involve storage of renewable energy (solar thermal energy), and are space efficient as they are underground (Başer and McCartney 2015a).

Despite the successful use of SBTES systems in community-scale applications (Sibbitt et al. 2012; Nussbicker-Lux 2012; Bjoern 2013), there are still opportunities for engineers to improve the performance of SBTES systems by considering the role of the hydrogeological setting in the subsurface. A goal of this study is to understand the benefits of installing SBTES systems in the vadose zone, the layer of unsaturated soil or rock near the ground surface that may extend to depths greater than 10 meters in some locations. The unsaturated porous material in the vadose zone has a lower thermal conductivity than when saturated, limiting the transient spreading of heat away the subsurface heat storage system (Choi et al. 2011). The volumetric heat capacity of soils in unsaturated conditions is lower than in saturated conditions but is still greater than in dry conditions. For example, the volumetric heat capacity of a silty soil is 2.5 MJ/m^{3}K for saturated conditions, 2.0 MJ/m^{3}K for a degree of saturation of 0.5, and 1.2 MJ/m^{3}K for dry conditions (Baser et al. 2016d). One challenge is that the modes of heat transfer in unsaturated porous materials are more complex than when dry or water-saturated. Specifically, in addition to coupling between the thermal and hydraulic properties of unsaturated soils and the effects of temperature on fluid properties (e.g., Lu and Dong 2015), the modes of heat transfer in unsaturated soils include a combination of conduction, convection due to the flow of pore water in liquid and vapor forms under thermal and hydraulic gradients, and latent heat transfer due to phase change. Several studies have developed models to capture these different mechanisms of coupled heat transfer and water flow in unsaturated soils, and have applied them to problems associated with radioactive waste repositories (e.g., Ewen and Thomas 1989; Thomas and Sansom 1995; Gens et al. 1998; Gens et al. 2009), soil-atmosphere interaction (Smits et al. 2011), energy piles (Akrouch et al. 2016), and borehole geothermal heat exchangers (Başer et al. 2018). Başer et al. (2018) found that the zone of influence of temperature changes in silt around a heat exchanger were greater for unsaturated conditions when considering the impact of vapor phase convection. Previous simulations of geothermal heat exchangers in unsaturated soil used conduction alone with a thermal conductivity that varies with the initial degree of saturation (e.g., Choi et al. 2011), but Başer et al. (2018) found that thermally-induced water flow may lead to significant differences in the thermo-hydraulic response of the subsurface.

This paper presents a comparison of transient changes in ground temperatures measured in a field-scale SBTES system installed in the vadose zone in San Diego, California with those predicted from a numerical model for coupled heat transfer and water flow. The testing program involved a 4-month period where heat collected from solar thermal panels was injected into the borehole array, followed by a 5-month ambient cooling period. Heat transfer rates into the subsurface measured in the field-scale SBTES system were used to define the dynamic boundary conditions for heat injection in the model, considering the effects of fluctuations in surface air temperature. Although the primary variable from the comparison is the ground temperature, the numerical model also permits evaluation of the effects of thermo-hydraulic interaction between the closely-spaced boreholes in the SBTES system on the degree of saturation. This is important as changes in the degree of saturation due to thermally-induced water flow may lead to associated changes in the subsurface thermo-hydraulic properties of unsaturated soils.

2. BACKGROUND

Since the concept of borehole thermal energy storage systems was introduced by Claesson and Hellström (1981), several SBTES systems have been installed in Canada and Europe as part of district-scale heat distribution systems. The Drake Landing SBTES system in Okotoks, Alberta, Canada supplies heat from solar thermal panels installed on garage roofs to an array of 144 boreholes in a 35 m-deep, 35-m wide grid (Sibbitt et al. 2012), which is then used to supply approximately 90% of the heat demand of 52 homes. Catolico et al. (2016) simulated the response of the Drake Landing SBTES system, which lies in water-saturated sand deposits overlying glacial till, using a numerical model in TOUGH2 using time-dependent injection fluid temperatures measured at the site over six years of operation as the main boundary condition. Over each year of operation, lateral heat transfer from the borehole array to the surrounding ground was found to decrease due to a reduction in the thermal gradient between the center of the array and the surrounding subsurface, meaning that more thermal energy was concentrated in the center of the array. They found that the annual efficiency of heat extraction (heat extracted divided by heat injected) increases over time, approaching a value of 55%. However, the efficiency of heat recovery was found not to be a good quantification of the SBTES performance because if the demand for heat in a given winter is lower the the efficiency will decrease. Instead, it may be better to evaluate the fractions of heat injected, stored, and lost. For example, in the 6th year of operation, 31.5% of the heat injected into the system was recovered, 21.9% of the heat injected remained in the borehole array, and 46.7% of the heat injected escaped the borehole array. Despite the seemingly high fraction of heat loss, the heat stored and recovered was sufficient to provide more than 90% of the community's annual heating demands. Another successful SBTES system was installed in 2007 is in Braedstrup, Denmark (Bjoern 2013). This system supplies heat from 18,000 m^2 of solar thermal panels to an array of 50 boreholes having a depth of 47 to 50 m installed across a 15 m-wide area. This system provides 20% of the heat to 14,000 homes. Another commercial-scale SBTES was installed in 2008 in Crailsheim, Germany involving of a series of 55 m-deep boreholes that formed a 39,000 m^3 subsurface storage volume. This system stores heat from 7410 m^2 of flat plate solar thermal collectors to provide heat for a school and 230 dwellings (Nussbicker-Lux 2012).

Although the experience from the commercial-scale systems at Drake Landing, Braedstrup and Crailsheim indicates that SBTES systems are functional and are sufficiently efficient to provide heating to different sizes of communities, simulation studies such as that of Catolico et al. (2016) indicate that the hydrogeological setting is critical for optimizing the thermal energy storage. Although the Drake Landing SBTES system includes instrumentation to evaluate changes in ground temperature within the array (Sibbitt et al. 2012), it is in use for commercial purposes, so the heat injection patterns cannot be varied as part of scientific studies on the performance of SBTES systems. Accordingly, it is advantageous to install smaller SBTES systems for demonstration projects in different hydrogeological settings to understand the roles of different heat transfer processes and heat injection patterns on SBTES system performance. For example, Başer et al. (2016a) reported the ground temperatures monitored during a 75-day heat injection experiment into a small-scale SBTES system in Golden, CO, USA involving an array of 5 borehole heat exchangers. Although the SBTES system in that study was installed in an unsaturated silty soil layer, observations during installation indicate that the bottom 10% of the heat exchanger lengths were in a saturated sand aquifer underlying the site. Transient temperature measurements indicated that a substantial portion of the injected heat left the array due to lateral heat loss associated with both the higher thermal conductivity of the saturated sand layer and possible convection effects associated with groundwater flow in this sand layer. Further, the simulations of Başer and McCartney (2015b) indicate that arrays should have a greater number of boreholes than those considered by Başer et al. (2016a) to effectively concentrate heat in the subsurface.

Although simplified design models for SBTES systems have been developed (e.g., Claesson and Hellström 1981), modeling the transient heat transfer in SBTES systems can be complex because of the dimensions of the problem, the geometry and structure of the borehole network, the process of heat transfer into the ground via circulating fluids in closed-loop pipe networks, and the nonlinear variations in the thermal and hydraulic properties of unsaturated soils with degree of saturation. Marcotte and Pasquier (2014) investigated the effect of the borehole arrangement both analytically and numerically on the thermal response of a heat storage system for the cases in which boreholes are connected in series, parallel, and mixed configurations. They reported significantly lower inlet fluid temperatures for the parallel configuration than for the series configuration, indicating a larger heat transfer to the ground for this arrangement compared to the series configuration. Besides the geometrical configuration of the borehole heat exchangers and the fluid circulation configuration (series, parallel, mixed), there are other factors that affect the thermal response of a storage system, such as the subsurface temperature profile and ambient air temperature, degree of saturation profile of soil and the thermal properties. Thomas and Rees (2009) investigated the effect of water content on heat transfer through unsaturated soils via a series of one and two-dimensional numerical simulations that consider only conduction as the major heat transfer mechanism. They reported 60% and 20% increases in heat flux with increasing water content for one- and two-dimensional models, respectively. Akrouch et al. (2016) proposed an analytical solution based on cylindrical heat source theory that accounts for variable degree of saturation on the heat exchange between the heat source and sand soil and the results indicated a 40% drop in performance of a heat exchanger when the degree of saturation is close to residual conditions. Welsch et al. (2015) studied the impact of borehole length, borehole, spacing, number of boreholes, and the inlet heat transfer fluid temperatures on the behavior of thermal energy storage in crystalline rock. They observed that there was an optimal spacing to reach the highest efficiency of heat recovery, with higher and lower values leading to lower efficiencies. Due to the high thermal conductivity of the crystalline rock, the optimal borehole heat exchanger spacing was 5 m, which is greater than that observed in similar studies the focus on lower thermal conductivity soils (e.g., Baser and McCartney 2015a). Welsch et al. (2015) found that the number of boreholes has a positive influence on the efficiency of heat recovery because the increasing ratio of the storage volume to the size of the boundary of the storage volume results in lower heat losses to the surrounding subsurface outside of the array.

Başer and McCartney (2015a) used a conduction-only model to understand the impacts of borehole array geometry, ground properties, heat injection magnitudes, and heat injection duration on the temperature distribution in the SBTES system. Başer et al. (2016b) and Başer et al. (2016c) used a coupled heat transfer and water flow model without considering vapor diffusion or phase change to understand the roles of incorporating a thermal insulation layer and the effect of different unsaturated soil properties on the ground temperatures in SBTES systems, respectively. These studies found that a surface insulation layer does not play a significant role on the thermal energy storage due to the small area around each borehole heat exchanger, but that surface temperature fluctuations should still be considered on the ground temperatures. Bidarmaghz et al. (2016) investigated the effect of surface air temperature changes on the thermal response of geothermal heat exchangers in the shallow subsurface and found that considering ambient air temperatures in the simulations increased the total heat exchanger length by 11%. A similar study by Nguyen et al. (2017) showed that seasonal temperature variation of the subsurface increases the outlet fluid temperature causing a decrease in the heat transfer rate into the ground. Further, they found that burying boreholes at the certain depth from the surface (1-2 m) is not sufficient to hinder the ambient air temperature effects on the ground temperature near the surface. Baser et al. (2017) used a coupled heat transfer and water flow model considering vapor diffusion and phase change to study the response of a single vertical borehole heat exchanger during a heat injection period followed by a, ambient cooling periods. They evaluated the role of different heat transfer mechanisms and observed a permanent drying around the heat exchanger during heat injection that was not recovered during ambient cooling. This drying led to a decrease in thermal conductivity that corresponded to a reduction in the amount of heat loss from the soil near the heat exchanger.

3. NUMERICAL MODEL

3.1. Model Formulation

This study applies the model for geothermal heat exchangers in unsaturated soils used by Baser et al. (2018), which was originally developed by Smits et al. (2011) and enhanced by Moradi et al. (2016), to simulate the behavior of a field-scale SBTES system installed in San Diego, California. The governing equations for the model are summarized in Table 1, while the key thermo-hydraulic constitutive relationships are summarized in Table 2. Coupling occurs between the different equations in Table 1 due to the effects of temperature on the different fluid properties, which are summarized by Smits et al. (2011) and Baser et al. (2018). Simulation of coupled heat transfer and water flow in unsaturated soils requires simultaneous solution of the governing equations for two-phase flow (Equations 1 and 2) along with the heat transfer based on energy balance (Equation 6). Because liquid and vapor phases are present in unsaturated soils, flow induced by thermal gradients in both liquid and total gas phases are considered and formulated as the convection terms in the energy balance equation (i.e., the second and the third terms in Equation 6). When formulating the model, some assumptions are made: (a) soil framework is homogeneous, isotropic, and non-deformable; (b) fluid phases are immiscible; (c) hysteresis in the constitutive relationships is not considered. The model considers enhanced vapor diffusion described by Equation (4) and a nonequilibrium phase change rate described by Equation (5) that are incorporated into the water vapor mass balance equation in Equation (3) and as source terms in the governing equations for two-phase flow and the heat transfer energy balance. The model was implemented into the finite element-based software COMSOL Multiphysics® version 5.2a (COMSOL 2015) which solved the governing equations for the four primary unknowns: pore water pressure, total pore gas pressure, water vapor concentration, and temperature.

3.2. Model Calibration

The key parameters that must be defined to calibrate the numerical model are the parameters of the thermo-hydraulic constitutive relationships given in Table 2 and the parameters *a* and *b* from Table 1 that govern the soil-specific enhanced vapor diffusion rate and the nonequilibrium phase change rate, respectively. The methodology described in this section for parameter calibration was applied to the subsurface in the SBTES array evaluated in this study but could also be applied to design SBTES systems in the vadose zone in other locations.

The SBTES system constructed as part of this study was installed in an unsaturated conglomerate bedrock layer at the Englekirk Structural Engineering Center (ESEC) of the University of California San Diego. A site investigation from 2003 indicates approximately 1m of sandy soil overlying the conglomerate bedrock consisting of cemented sand- and gravel-size particles. An undisturbed core of the conglomerate bedrock was not obtained during installation of the SBTES system. However, disturbed cuttings from a hole drilled into the conglomerate using an auger were collected from different depths. Although it is not possible to reconstitute the cuttings into the same cemented structure as the conglomerate, it is assumed that the thermo-hydraulic properties of the conglomerate are predominantly governed by the grain size, mineralogy, and density for the purposes of model calibration so that laboratory calibration of the model parameters is possible. Laboratory calibration permits the use of instrumented specimens under carefully-controlled boundary conditions, but future studies may use inverse analyses from field measurements to consider the role of the cemented structure on the calibrated model parameters. Specimens used to represent the conglomerate properties were reconstituted from cuttings obtained from a depth of 16 m from the surface at the ESEC facility, which were prepared using compaction to a dry density of a 1650 kg/m^3 at an initial degree of saturation of 0.49, which corresponds to conditions in the conglomerate measured using sand-cone experiments performed at a depth of 1.5 m from the surface.

The thermo-hydraulic constitutive relationships were determined using a modified form of the transient water release and imbibition method (TRIM) of Wayllace and Lu (2012) that included the measurement of the thermal conductivity and volumetric specific heat capacity described by Lu and Dong (2015). Specifically, a specimen was compacted to the conditions mentioned above into a modified Tempe cell that incorporates a dual thermal needle and a dielectric sensor, was saturated with water, then dried monotonically in two stages. The soil water retention curve (SWRC), hydraulic conductivity function (HCF), thermal conductivity function (TCF), and volumetric heat capacity function (VHCF), described by Equations 7 through 10 in Table 2, were obtained from inverse analysis of the outflow and thermal property measurements during this drying stage. The SWRC and HCF along with relevant parameters are shown in Figure 1(a), while the TCF and VHCF along with relevant parameters are shown in Figure 1(b). Lu and Dong (2015) presented empirical relationships between the parameters of the thermal constitutive relationships and the hydraulic constitutive relationships, but the properties measured from the experiments in Figure 1 were used in the simulations.

The properties governing the vapor diffusion phase change rate and diffusion were calibrated using an evaporation experiment on a reconstituted specimen of the site soil. The soil was compacted in a plastic modified Proctor compaction mold having a diameter of 152 mm to a height of 179 mm. The mold, developed by Iezzoni and McCartney (2015), can accommodate a dielectric sensor at mid-height of the soil specimen as shown in the cross-sectional schematic in Figure 2. An evaporation test starting from the initial degree of saturation mentioned above was performed by heating the bottom of the soil layer using a heating pad placed below the mold while leaving the surface of the soil open to the atmosphere. The heating pad applies fluctuating heat pulses to maintain a target temperature. Thus, a thermocouple was placed at the bottom to monitor the applied boundary temperature during heating, which is shown in Figure 3(a). Ambient temperatures were also recorded with a thermocouple so that the ambient air temperatures could be applied as boundary conditions on the outer surfaces of the specimen during the experiment. A temperature of approximately 42 °C was maintained over a period of 35 h. The measured values of temperature and degree of saturation at the center of the soil specimen during this period are shown in Figures 3(a) and 3(b), respectively. The model of Iezzoni and McCartney (2015) was used to correct the degrees of saturation inferred from the dielectric sensor to account for temperature effects. This calibration test was then simulated using the coupled heat transfer and water flow model, and the parameters *a* and *b* in Equations 4 and 5 in Table 1 were varied using a manual parameter sweep to identify the best combination of parameters to match the measured curves. The simulated temperature and degree of saturation curves for $a = 20$ and $b = 2\times10^{-7}$ s/m^2 are shown in Figures 3(a) and 3(b), respectively, which indicate a good match.

3.3. Simulation Details for the Field-Scale SBTES System

The calibrated model was then used to simulate the response from the field-scale SBTES system demonstration experiment. A plan view of the SBTES system showing the connections between the boreholes in the array, a manifold for control and monitoring of the heat exchanger fluid in the borehole array, a 2400 L water-filled temporary heat storage tank, and a series of solar thermal panels is shown in Figure 4(a). This figure also shows the location a reference borehole for monitoring the undisturbed ground temperature profile. Thirteen of the boreholes in the array include heat exchanger tubing, while four of the boreholes in the array include thermistor strings that monitor the ground temperature. Two of the boreholes include both heat exchangers and thermistor strings. The boreholes were backfilled with sand bentonite after installation of the heat exchangers or thermistor strings. The hexagonal configuration of the borehole array was selected for ease of construction, as the boreholes in the array fall into five co-linear sets that facilitate positioning of the drill rig. The main design variable used to configure the boreholes was the spacing. Baser and McCartney (2015a) found that the borehole spacings should be less than 1.5 m to ensure overlapping effects of the heat exchangers for soil thermal properties and heat transfer rates typical of SBTES systems. The number of boreholes containing heat exchangers was selected so that the boreholes in the array would fall into two annuli, greater than the number in the array tested by Baser et al. (2016a). Although a commercial-scale SBTES system would likely have more heat exchangers in several more annuli (e.g., Sibbitt et al. 2012), this array is still sufficient in scale to investigate the transient heat transfer and heat storage in the subsurface within the array associated with interactions between heat exchangers.

An elevation view of the site is shown in Figure 4(b), which highlights the position of the 15 m-long boreholes beneath a 1 m-deep excavation. After connection of the heat exchanger tubing following the arrangement shown in Figure 4(a), a thin layer of site soil was placed for leveling-purposes, which was overlain by a hydraulic barrier, an insulation layer, and a compacted layer of site soil. The high-density polyethylene (HDPE) hydraulic barrier has a thickness of 0.01 m and an assumed hydraulic conductivity of 10^{-12} m/s, while the EPS geofoam insulation layer has a thickness of 50 mm, a thermal conductivity of 0.03 W/mK, and a specific heat capacity of 0.9 MJ/kgK. The lateral extents of the hydraulic barrier and insulation layer followed the hexagonal boundaries of the array shown in Figure 4(a). Pictures of the SBTES system are shown in Figure 5, highlighting the 1 m-deep excavation and connection of the borehole heat exchangers in Figure 5(a), the hydraulic barrier in Figure 5(b), the insulation layer in Figure 5(c), and the completed set of solar thermal panels and temporary heat storage tank in Figure 5(d).

As the hexagonal borehole array is symmetrical, a quarter section was simulated as shown in Figure 6. The temperatures on either side of the two planes of symmetry are assumed to be identical. This simulation strategy was also used by Catolico et al. (2016) to reduce computation times when simulating symmetrical SBTES systems. Figure 6 also includes the labels used to name the thirteen boreholes that include heat exchangers (boreholes A through M) and the four boreholes that include thermistor strings (T-1 to T-4). As will be described below, appropriate fractions of the heat transfer from boreholes A (1/4 of its heat transfer), B (1/2 of its heat transfer) and E (1/2 of its heat transfer) are applied as boundary conditions. The model domain is 15 m x 15 m in plan and has a depth of 20 m and includes 5 borehole heat exchangers. The size of the domain was selected such that the heat exchangers would not affect the temperatures at the boundaries for the heat injection period under investigation. This was confirmed by ensuring that the temperature at the boundaries of the array remained similar to the temperatures from the reference borehole at different depths. The domain was discretized using 756,667 elements with finer discretization around the boreholes. Triangular elements were used on the surfaces of boreholes and insulation layer, and tetrahedral elements were used for the rest of the domain. A maximum element growth rate of 1.4 and a curvature factor of 0.25 were used in discretization in COMSOL.

The isometric views of the model domain shown in Figures 7(a) and 7(b) highlight the thermal and hydraulic boundary and initial conditions, respectively. The initial temperature profile was obtained from the ground temperature distribution measured by the reference borehole at the initiation of the heat injection period on April 29th, 2016. To define the initial degree of saturation profile, hydrostatic conditions were assumed. Although the water table was not encountered in the previous geotechnical site investigation which was performed in 2003, the San Diego County Water Authority reported that the ground water depth ranges in depth from 14 to 24 m in the area and no groundwater flow was recorded. Accordingly, the water table was fixed at a depth of 20 m from the surface (i.e., at the base of the domain) throughout the simulations for simplicity as its actual location during the experiment is unknown. Although the depth of the groundwater table may be greater than 20 m, this choice of boundary condition was selected to limit the size of the domain in the simulations. Based on the hydrostatic profile shown in Figure 7(b), the initial degree of saturation along most of the length of the heat exchangers was approximately 0.22 which corresponds to residual saturation conditions. Near the bottom of the heat exchangers, the initial degree of saturation increases up to 0.49 due to the proximity of the water table.

Neumann boundary conditions of zero mass flux and zero heat flux were assigned for the outer lateral boundaries of the domain as well as for the planes of symmetry. Dirichlet boundary conditions for temperature were applied at the bottom and top of the domain. A constant temperature of 21°C was applied at the bottom of the domain, which corresponds to the average measured temperature at the base of the reference borehole. The temperature of the top of the domain was assumed to equal the time-dependent ambient air temperatures that were measured at the site during the duration of the experiment, shown in Figure 8(a). Although the EPS geofoam insulation layer is considered in the simulations, it does not provide a perfect insulation effect so the effects of the ambient air temperature fluctuations on the surface temperature must be considered. It should be noted that the surface ground temperature may differ from the ambient air temperature due to radiative and air convection effects, so the use of the ambient air temperature as a surface boundary condition may be a simplifying assumption. A zero-mass flux boundary condition was applied to the surface boundary. This choice was made to simplify the fluid flow processes in the ground as an infiltration/evaporation boundary condition can be computationally expensive when combined with a coupled heat transfer and water flow model considering vapor diffusion and phase change. However, this assumption is reasonable both due to the relatively low precipitation in San Diego as well as due to the presence of the hydraulic barrier atop the borehole array. However, this boundary condition choice is expected to affect the accurate simulation of the temperature at the location of the reference borehole, as infiltration of water may affect the thermal properties of the surface soil. As mentioned, Dirichlet boundary conditions were assumed for the water table at the base of the domain (pore water pressure equal to zero).

Although the heat transfer boundary conditions for geothermal borehole heat exchangers previous simulations of SBTES systems involved control of the inlet fluid temperature and considered convective heat transfer associated with fluid flow through the sequence of borehole heat exchangers in the array (e.g., Welsch et al. 2015; Catolico et al. 2016), this study considered the borehole heat exchangers as cylindrical heat sources and applied heat flux values to the outer diameters of the cylinders equal to the measured heat flux values from the site discussed in the next paragraph. The heat transfer boundary conditions associated with fluid flow through heat exchanger pipes were not considered in this study because of long computational times associated with solving the governing equations for coupled heat transfer and water flow processes in the subsurface given in Table 1, which was the primary topic of interest in this study. The simplified heat transfer boundary condition for the borehole heat exchangers still permits validation of the coupled heat transfer and water flow analyses in the subsurface within the array. However, design simulations for SBTES systems require control of the inlet fluid temperature and consideration of convective heat transfer of fluid flow through the heat exchangers as the heat transfer rate will decrease over time as the soil within the array increases in temperature (e.g., Welsch et al. 2015). Another assumption in this study is that a uniform heat flux was applied to each of the heat exchangers based on the measured heat transfer rates in the field. Although the choice of a uniform heat flux along a heat exchanger connected in series through several boreholes may not be suitable when simulating a commercial-scale SBTES system with long overall heat exchanger lengths, the relatively short overall heat exchanger lengths used in this field demonstration project permitted the use of this simplified boundary condition without major discrepancies in matching the measured subsurface temperatures.

Eight evacuated tube solar thermal panels having a total area of 33 m^2 were connected in series to collect heat during the day, which was then transferred to the water in the temporary heat storage tank via a coiled copper tube. A second coiled copper tube in the temporary heat storage tank is used to inject heat into the SBTES system. A second horizontal SBTES system was also installed at the site and was tested at the same time (Baser et al. 2019). Although this horizontal SBTES system is not discussed in this paper, it should be acknowledged as all the heat collected from the solar thermal panels was not injected into the “vertical” SBTES system under evaluation in this study. Nonetheless, the measured heat transfer rate into the subsurface was boundary condition used in the simulations, so the effects of the horizontal SBTES system is not important. Water was used as the heat exchanger fluid in both the solar thermal panels and in the SBTES system as freezing temperatures are not expected in San Diego. The heat transfer rates were calculated as follows:

$$\dot{Q} = \dot{V}_w \rho_w C_w \left(T_{in} - T_{out}\right) \tag{11}$$

where $\dot{V}_w$ is the measured volumetric flow rate of the heat exchanger fluid (water), ρ_w is the density of water (1000 kg/m^3), C_w is the specific heat capacity of water (4183 J/kgK), and T_{in} and T_{out} are the measured temperatures of the water entering and exiting solar thermal panels, respectively. The heat transfer rates for the solar thermal panels over the 120-day period starting on April 29, 2016 are shown in Figure 8(b). The large fluctuations in heat transfer rate observed in this figure occur because heat is only collected during the day. To better understand the transient heat transfer rates from the solar thermal panels and the total heat injected into the vertical SBTES system during 2 days of operation are shown in Figure 8(c). A lag is observed between the heat transfer rates collected from the solar thermal panels and injected into the vertical SBTES, but the temporary water storage tank provides a buffer to permit heat injection at night as well. A control system has not yet been implemented to ensure that heat is only collected from the solar thermal panels during the day. Specifically, the circulation pumps in the solar thermal panels and SBTES system are operated continuously. Accordingly, fluid is still circulated through the solar panels at night, which may result in a slight extraction of heat from the temporary heat storage system if the outside air is colder than the borehole array. The efficiency of heat transfer in the system can be assessed using the cumulative total energy collected from the solar thermal panels and injected into the vertical and horizontal SBTES systems shown in Figure 8(d). Approximately 80% of the cumulative heat collected from the solar thermal panels is injected into the vertical and horizontal SBTES systems, with the remaining 20% lost due to the circulation of fluid through the solar thermal panels at night. Additional experimental testing is underway to investigate other configurations for flow through the solar thermal panels (series instead of parallel) along with inclusion of a heat transfer fluid control system in the solar thermal panels to increase the efficiency of heat collection from the solar thermal panels and injection into the SBTES systems.

As mentioned, the borehole heat exchangers were simulated as cylinder sources having a uniform heat flux with depth with a magnitude that varied according to the measured heat flux interpreted from Equation (11) using the entering and exiting fluid temperatures and fluid flow rates going into the different geothermal loops shown in Figure 4(a). Specifically, the heat exchanger tubing was split into three closed-loop networks of U-tube borehole heat exchangers (referred to as Loops 1, 2, and 3). Each loop is connected to a borehole heat exchanger in the central borehole, which means that the central borehole contains 3 U-tube heat exchangers. Next, the three loops connect to four other borehole heat exchangers in different zones of the array, as shown in the photograph in Figure 9 and the schematic in Figure 4(a). It is expected that the heat exchanger fluid flowing through the loops will be hottest in the center of the array, and the fluid temperature will decrease as it flows through the surrounding four borehole heat exchangers and returns to the manifold. However, as noted above, the relatively short length of the heat exchangers in each loop permits the assumption that the heat flux is the same from each borehole connected to the loop (except for the central borehole which has three times the other boreholes). The use of three loops provides flexibility for changing the heat transfer into different zones of the array, but in this study all three loops had a balanced flow. Specifically, the fluid flow rates in each of the loops were controlled and measured independently to be equal and ensure that heat transfer is balanced into the different zones of the borehole array. The inlet and outlet fluid temperatures for each loop were monitored so that Equation (11) could be applied to obtain the heat transfer rate into the subsurface, which was the main boundary condition applied in the simulations.

A challenge encountered when simulating a quarter domain is that boreholes from different loops were included in the domain, and the heat transfer rates in each loop were not the same. Specifically, the borehole heat exchangers that were simulated were A (center borehole, part of loops 1, 2, and 3), B (part of loop 2), C (part of loop 2), and D (part of loop 3), E (part of loop 3) as shown in Figure 9 and Figure 4(a). Further, the heat transfer rates calculated using Equation 11 represent an average heat transfer rate across the five borehole heat exchangers in each loop. Accordingly, some assumptions had to be made regarding the heat transfer rates applied to the different borehole heat exchangers being simulated. Because the different borehole heat exchangers were obtained from different loops, the heat transfer rates for the different borehole heat exchangers were interpreted from the heat transfer rates of Loops 1, 2, and 3 calculated from Equation 11 which are shown in Figure 10. Specifically, the total heat transfer rates from all three loops were first divided by five to represent the heat transfer rate into the five boreholes in the quarter section domain and the transient heat fluxes were applied to each borehole individually depending on its associated loop. The heat transfer rate for the center borehole was equal to the sum of 1/5th of each of the three heat transfer rates, and the heat transfer rates for boreholes B, C, D, and E were equal to 1/5th of the heat transfer rates from the respective loops noted above. Although it is likely that the center borehole A had a higher local heat flux than the outer borehole E it is assumed that the gradients of temperature in the center and edge of the array balanced out over time, so the total heat transfer rate of each loop could be considered as an average of the entire system. The transient heat transfer rates were converted to heat fluxes which were applied to the outside area of each borehole in the quarter section domain. At the end of the heat injection period, the heat flux for each borehole was set to zero to represent the ambient cooling period. Because the coupled heat transfer and water flow processes in the subsurface are relatively slow, a time interval of 1800 s was used in the simulations of the 120-day heat injection period followed by a 155-day ambient cooling period, which was found to lead to sufficiently accurate results when evaluating the changes in ground temperature.

4. COMPARISON OF NUMERICAL RESULTS AND FIELD MEASUREMENTS

A goal of this study is to present the field measurements in a way that the transient heat transfer results at different locations in the borehole array could be understood. Second, because of the simplifying assumptions regarding the subsurface thermo-hydraulic properties (homogeneity and use of reconstituted specimens), the uncertain location of the water table below the heat exchanger array, and the use of a uniform heat flux along the boreholes, it is preferred to show a qualitative comparison between the field measurements and the results from the numerical simulation without a detailed error analysis.

As could be expected from the large fluctuations in the heat transfer rate into the geothermal heat exchanger loops due to the variability in the solar thermal heat transfer rate, the temperature at the locations of the borehole heat exchangers are expected to experience significant changes in temperature each day. The temperatures at the center borehole measured using the thermistor string T-1 along with the simulated temperature from the model are shown in Figure 11. The temperature at each depth is shown separately in each sub-figure to differentiate the transient response at the different depths. Although the temperatures at a depth of 16.00 m were underestimated during heating, the temperatures at other depths were captured well by the model. The difference at a depth of 16.00 m may be due to the assumption of the hydrostatic initial conditions based on the assumed location of the water table, which leads to a higher thermal conductivity of the subsurface in the simulations. The differences in the daily fluctuations of each depth occur as the temperatures from the model were obtained in a soil element at the boundary of the heat exchanger, while the measured temperatures are from the thermistor strings inside the borehole and are in contact with the geothermal heat exchanger. The sand-bentonite grout backfill in the boreholes was not considered in the model simulations but may affect the heat transfer process in the field measurements. During the ambient cooling stage, the transient trends appear to be well-captured, although the initial temperature at the start of ambient cooling was occasionally different from that between the measured and simulated values. The two locations closer to the surface show an increase in the rate of cooling on day 210, likely due to the lower ambient air temperatures observed in Figure 8(a).

A comparison between the temperatures at the location of thermistor string T-2 shown in Figure 12 indicates less daily fluctuations than at the location of thermistor string T-1. The temperature at the location of thermistor string T-2 depends on overlapping effects of borehole heat exchangers A and B, and heat transfer from these boreholes damps out the daily fluctuations. A good match in the trends and magnitudes at the different depths was observed during both the heat injection and ambient cooling periods, with underestimation of the temperatures at depths of 16.00 m and 1.82 m. The measured temperature values during the heating injection period ranged from 29.5 °C near the bottom of the array to 34.2 °C near the top of the array. The greater increases in measured and simulated temperatures near the surface of the array may be due to greater heat transfer in initially dryer soils due to greater water vapor diffusion and latent heat transfer as well as buoyancy-driven upward movement of water vapor, both of which were observed by Baser et al. (2018) in the simulation of a single geothermal heat exchanger. The measured and simulated temperatures at the location of thermistor string T-3 shown in Figure 13 are similar to those for thermistor string T-1 in Figure 11 due to the presence of borehole heat exchanger B, but with lower magnitudes. The lower magnitude is because the heat flux from borehole heat exchanger B was three times smaller than the three loops in borehole heat exchanger A. Finally, the measured and simulated temperatures at the location of thermistor string T-4 shown in Figure 14 show the lowest increases in temperature due to its larger radial location from the center of the borehole array. One of the thermistors at a depth of 12.95m was not functional after installation. Like thermistor string T-2, greater temperatures were noted near the surface.

The differences between the simulated and measured ground temperatures could be due to the use of reconstituted specimens to obtain the thermo-hydraulic properties, the possibility that the subsurface does not have homogeneous thermo-hydraulic properties, uncertainty about the actual depth of the groundwater table (which may have affected the initial degree of saturation and thermal properties), and the use of simplified heat exchanger boundary conditions. A general observation regarding the measured and simulated temperature time series is that even though the heat transfer was simulated as an average heat flux at the boundaries of the heat exchangers instead of simulating the heat transfer via circulation of fluid in the borehole loops, a good match with the ground temperatures during both heating and cooling was observed. Although the actual location of the water table was not known a-priori, comparison of the simulation results shown in Figures 11 through 14 at depths near the middle and bottom of the heat exchangers indirectly reflect the importance of the initial degree of saturation on the simulation results from the coupled heat transfer and water flow model. Greater initial degrees of saturation will lead to higher thermal conductivity values and may lead to greater changes in degree of saturation due to enhanced vapor diffusion and latent heat transfer (Baser et al. 2018). The differences in simulated and measured temperatures at the different depths in the soil profile in Figures 11 through 14 could also have been due to variations in subsurface stratigraphy not observed in the installation of the heat exchangers, which would have led to variations in thermo-hydraulic properties with depth. Despite the challenges in validating the numerical model with field data, the numerical model was found to capture the temperature of the subsurface within the array with good accuracy within most of the array.

Radial profiles of temperatures at the end of the heat injection period from the numerical model and the field measurements are shown in Figures 15(a) for the depths that thermistors were installed. Temperatures were in good agreement, especially at depths of 14.78 and 1.82 m. This figure also includes the ground temperatures from the reference borehole. The shapes of the radial profiles are like those interpreted from the field measurements, although the maximum temperatures at the locations of thermistor strings 1 and 3 due to the daily fluctuations in heat transfer rate were not captured as noted in the time series in Figures 11 and 13, respectively. Radial distributions in temperature at the end of the ambient cooling period indicate that some heat (a maximum difference in temperature of 4 °C from the initial value of 21 °C) is still retained within the array after 5 months of ambient cooling. This amount of decrease in temperature due to ambient cooling is expected to decrease if further cycles of heating and cooling were investigated, similar to the observations of Catolico et al. (2016). Temperature profiles at the locations of boreholes 2 and 4 are shown in Figures 16(a) and 16(b), respectively. Both the measured and simulated temperature profiles show an increase in temperature with proximity to the ground surface, likely due to the effects of natural convection. As the pore fluids are heated, their densities decrease causing them to rise and transfer heat upward in the subsurface.

5. ADDITIONAL INSIGHTS FROM MODEL SIMULATIONS

Although it was known that the subsurface at ESEC was unsaturated, and that changes in degree of saturation are expected due to coupled heat transfer and water flow, instrumentation was not incorporated in the subsurface within the borehole array to monitor changes in degree of saturation. This was due to difficulty in installing dielectric sensors into the intact conglomerate through the sides of the boreholes. Installation of these sensors into a soil-bentonite-backfilled borehole would measure the changes in thermo-hydraulic behavior of the backfill, not the conglomerate. Nonetheless, it is still possible to infer the changes in degree of saturation of the subsurface from the numerical simulation results, as well as the effects of these changes on the heat transfer during the heat injection period and heat retention during the ambient cooling period. Time series of the simulated degrees of saturation at the locations of thermistor strings 3 and 2 are shown in Figures 17(a) and 17(b). Due to the boundary conditions associated with borehole heat exchanger B next to thermistor string 3, a steady decrease in degree of saturation was noted during the heat injection period at this location in Figure 17(a). This decrease in degree of saturation is expected due to enhanced vapor diffusion from relatively hot regions to colder regions. During the ambient cooling stage, the degree of saturation at the location of thermistor string T-3 was not observed to recover. A similar observation was made by Baser et al. (2018) for a single borehole heat exchanger in compacted silt that had different thermo-hydraulic properties. The main effect of this decrease in degree of saturation is that the decrease in temperature at this location during ambient cooling should be slower due to the lower thermal conductivity associated with the permanent decrease in degree of saturation. An interesting observation is that this same decrease in degree of saturation during the heat injection period was not observed in Figure 17(b) at the location of thermistor string T-2, which was between borehole heat exchangers A and B. In fact, a slight increase in degree of saturation is observed, likely due to movement of water vapor away from these two heat exchangers to the cooler regions between.

The differences in behavior at the locations of thermistor strings T-3 and T-2 indicates that for this particular set of thermo-hydraulic soil properties in Figure 1, the zone of influence of degree of saturation changes is relatively limited in the conglomerate material. The effect of the changes in degree of saturation with heating can be further investigated using the numerical simulation results through the radial distributions in degree of saturation, thermal conductivity, and volumetric heat capacity at the end of the heat injection period shown in

Figures 18(a), 18(b), and 18(c), respectively. Decreases in all three variables are noticed at the end of heating, with greater decreases at the locations of the borehole heat exchangers. The radial distributions for degree of saturation differ from those for the temperature observed in Figure 15, which reflect a clear overlapping effect between the borehole heat exchangers. Zones of influence of changes in degree of saturation of approximately 0.3 m is observed around borehole heat exchanger A and of approximately 0.25 m is observed around borehole heat exchanger B, which was not sufficient to cause a significant overlapping effect between the two boreholes. Although not investigated, repeated cycles of heat injection and heat removal may leader to greater zones of influence. Similar to the observations of Baser et al. (2018), greater decreases in degree of saturation are observed for the locations with initially greater degree of saturation and for greater changes in temperature, due to the effects of enhanced vapor diffusion and phase change. Another interesting observation is that the percent decrease in the thermal conductivity in Figure 18(b) is greater than the percent decrease in the volumetric heat capacity in Figure 18(c). This has positive implications on the performance of the heat storage systems as the lower thermal conductivity is expected to lead to decrease in the heat loss from the system while the volumetric heat capacity reflects the total heat that can be stored in the soil for a given increase in ground temperature.

Another comparison that can be made is the difference in the simulations expected for the subsurface having thermo-hydraulic properties representative of unsaturated and saturated conditions. When the subsurface is saturated, the governing equations in Table 1 are significantly simplified. Heat transfer will occur primarily due to conduction, but natural convection of the pore water will occur due to decreases in the density of water with temperature. A comparison of the simulations for saturated and unsaturated conditions along with the measured ground temperatures are shown in Figure 19 for a depth near the upper-middle of the array at the location of borehole T-2. The temperature for saturated conditions are generally lower, although they tend to rise sharply near the end of the heat injection period, possibly due to upward water flow due to natural convection. Further comparisons of the model for saturated and unsaturated conditions are shown in Baser et al. (2018) for the case of a single geothermal heat exchanger.

6. CONCLUSIONS

This study focused on the simulation of transient heat transfer and water flow in a field-scale SBTES system installed in the vadose zone. A non-isothermal, coupled heat transfer and water flow model considering enhanced vapor diffusion and nonequilibrium phase change calibrated in the laboratory using reconstituted specimens collected from the field was validated by comparing simulated ground temperatures with those from field-scale SBTES system during both heat injection and ambient cooling. In general, a good match was obtained between the simulated and measured temperature data, reflecting the importance of considering coupled heat transfer and water flow when simulating SBTES systems installed in the vadose zone. During heat injection, ground temperatures were generally greater near the surface in the borehole array, likely due to heat transfer due to buoyancy-driven vapor flow. At the end of 5 months of ambient cooling, some heat was still retained within the array, indicating that further heat injection and cooling cycles would lead to a positive effect on the performance of this heat storage approach.

Differences between the simulation and measured data were likely due to differences in how the heat injection boundary conditions were applied, the assumption of a homogenous subsurface, the calibration of the model parameters using reconstituted specimens, and the assumption regarding the depth of the water table (which may vary with time). Heat transfer led to a clear overlapping effect between the closely-spaced geothermal borehole heat exchangers in the SBTES system. However, the simulation results indicate that a significant overlapping effect was not observed in terms of the changes in degree of saturation between the geothermal borehole heat exchangers. Permanent decreases in degree of saturation were observed at the locations of the geothermal heat exchangers, corresponding to a decrease in thermal conductivity, but similar decreases in these variables were not observed in the bulk of the subsurface between the geothermal borehole heat exchangers for the particular conditions at the site. Further study on the effects of heating and cooling cycles of SBTES systems in the vadose zone may better clarify the roles of thermo-hydraulic interaction between closely spaced geothermal borehole heat exchangers for different subsurface materials.

ACKNOWLEDGEMENTS

Funding provided by National Science Foundation grant 1230237 is much appreciated. The opinions presented here belong to authors alone.

REFERENCES

Akrouch, G.A., Sánchez, M., and Briaud, J.L. (2016). “An experimental, analytical and numerical study on the thermal efficiency of energy piles in unsaturated soils.” Computers and Geotechnics. 71, 207-220.

Baser, T. and McCartney, J.S. (2015a). “Development of a full-scale soil-borehole thermal energy storage system.” Proc. Int. Foundation Conference and Equipment Exposition (IFCEE 2015). ASCE, Reston, VA. pp. 1608-1617.

Başer, T. and McCartney, J.S. (2015b). “Thermal energy storage in borehole arrays.” Symposium on Energy Geotechnics. Barcelona. Jun. 2-4. pp. 1-2.

Baser, T., Lu, N., and McCartney, J.S. (2016a). “Operational response of a soil-borehole thermal energy storage system.” ASCE Journal of Geotechnical and Geoenvironmental Engineering. 04015097-1-12. 10.1061/(ASCE)GT.1943-5606.0001432.

Baser, T., McCartney, J.S., Moradi, A., Smits, K., and Lu, N. (2016b). “Effect of a thermo-hydraulic insulating layer on the long-term response of soil-borehole thermal energy storage systems”. GeoChicago 2016: Sustainability, Energy and the Geoenvironment. Chicago. Aug. 14-18. ASCE, Reston, VA. pp. 125-134.

Baser, T., Dong, Y., and McCartney, J.S. (2016c). “Heat content in soil-borehole thermal energy systems in the vadose zone.” ICEGT 2016: 1st International Conference on Energy Geotechnics. Kiel. CRC Press, Boca Raton. pp. 195-202.

Baser, T., Dong, Y., Lu, N., and McCartney, J.S. (2016d). “Role of considering non-constant soil thermal parameters in the simulation of geothermal heat storage systems in the vadose zone”. Proceedings. 8th Asian Young Geotechnical Engineers Conference 2016 (AYGEC 2016). Kazakh Geotechnical Society. Astana. pp. 1-6.

Başer, T., Dong, Y., Moradi, A.M., Lu, N., Smits, K., Ge, S., Tartakovsky, D., and McCartney, J.S. (2018). “Role of water vapor diffusion and nonequilibrium phase change in geothermal energy storage systems in the vadose zone." Journal of Geotechnical and Geoenvironmental Engineering. 10.1061/(ASCE)GT.1943-5606.0001910.

Baser, T., Hanna, C., and McCartney, J.S. (2019). "Performance of a field-scale shallow horizontal thermal energy storage system." Geo-Congress 2019: The 8th International Conference on Case Histories in Geotechnical Engineering. Philadelphia, PA. Mar. 24-27. 1-10. Accepted.

Bear, J. (1972). Dynamics of Fluids in Porous Media. Dover, Mineola, N.Y., 764.

Bjoern, H. (2013). "Borehole thermal energy storage in combination with district heating." EGC 2013. Pisa. June 3-7. 1-13.

Bixler, N.E. (1985). NORIA: "A Finite Element Computer Program for Analyzing Water, Vapor, Air and Energy Transport in Porous Media." SAND84-2057, Sandia National Laboratories, Albuquerque, NM.

Campbell, G.S. (1985). Soil Physics with BASIC: Transport Models for Soil–Plant Systems. Elsevier, New York.

Campbell, G.S., Jungbauer, J.D., Bidlake, W.R., and Hungerford, R.D. (1994). "Predicting the effect of temperature on soil thermal conductivity." Soil Science. 158, 307–313.

Cass, A., Campbell, G.S., and Jones. T.L. (1984.) "Enhancement of thermal water vapor diffusion in soil." Soil Science Society of America. 48(1), 25–32.

Catolico, N., Ge, S., and McCartney, J.S. (2016). "Numerical modeling of a soil-borehole thermal energy storage system." Vadose Zone Hydrology. 1-17.doi:10.2136/vzj2015.05.0078.

Choi, J.S., Lee, S.R., and Lee, D.S. (2011). "Numerical simulation of vertical ground heat exchangers: Intermittent operation in unsaturated soil conditions." Computers and Geotechnics. 38, 949-958.

Claesson, J. and Hellström G. (1981). "Model studies of duct storage systems." New Energy Conservation Technologies and their Commercialization. J.P. Millhone and E.H. Willis, Eds. Springer-Verlag, Berlin. 762-778.

COMSOL Multiphysics® v. 5.2. (2015). COMSOL AB, Stockholm, Sweden.

Ewen, J. and Thomas, H.R. (1989). "Heating unsaturated medium sand." Géotechnique. 39(3), 455-470.

Gens, A., Garcia Molina, A., Olivella, S., Alonso, E.E., and Huertas, F. (1998). "Analysis of a full scale in-situ test simulating repository conditions." International Journal of Numerical and Analytical Methods in Geomechanics. 22(7), 515–48.

Gens, A, Sanchez, M., Guimaraes L., and Huertas, F. (2009). "A full-scale in situ heating test for high-level nuclear waste disposal: Observations, analysis and interpretation." Géotechnique, 59(4), 377-399.

Grant, S.A. and Salehzadeh, A. (1996). Calculations of temperature effects on wetting coefficients of porous solids and their capillary pressure functions. Water Resources Res. 32(2), 261-279.

Hillel, D. (1980). Fundamental of Soil Physics. Academic, San Diego, CA.

Iezzoni, H. M. and McCartney, J.S. (2016). "Calibration of Capacitance Sensors for Compacted Silt in Non-Isothermal Applications." Geotechnical Testing Journal, Vol. 39(2), 169-180.

Lide, D.R. (Ed.) (2001). Handbook of Chemistry and Physics, CRC Press, Boca Raton, FL.

Lu, N. and Dong, Y. (2015). “A closed form equation for thermal conductivity of unsaturated soils at room temperature.” Journal of Geotechnical and Geoenvironmental Engineering. 141(6), 04015016.

Marcotte, D. and Pasquier, P. (2014). “Unit-response function for ground heat exchanger with parallel, series or mixed borehole arrangement.” Renewable Energy. 68, 14–24.

McCartney, J.S., Ge, S., Reed, A., Lu, N., and Smits, K. (2013). “Soil-borehole thermal energy storage systems for district heating.” Proceedings of the European Geothermal Congress 2013. Pisa. Jun. 3-7. pp. 1-10.

Millington, R.J., and Quirk, J.M. (1961). “Permeability of porous solids.” Trans. Faraday Soc. 57, 1200–1207.

Moradi, A.M., Smits, K., Lu, N., and McCartney, J.S. (2016). “3-D experimental and numerical investigation of heat transfer in unsaturated soil with an application to soil borehole thermal energy storage (SBTES) systems.” Vadose Zone J. 15(10), 1-17.

Nguyen, A., Pasquier, P., and Marcotte, D. (2017). “Borehole thermal energy storage systems under the influence of groundwater flow and time-varying surface temperature.” Geothermics. 66, 110-118.

Nordell, B. and Hellström, G. (2000). “High temperature solar heated seasonal storage system for low temperature heating of buildings.” Applied Energy. 69(6), 511–523.

Nussbicker-Lux, J. (2012). “The BTES project in Crailsheim (Germany) – Monitoring results.” Proc. 12th Int. Conf. on Energy Storage – Innostock. IEA Press, Paris. 1-10.

Sibbitt, B., McClenahan, D., Djebbar, R., Thornton, J., Wong, B., Carriere, J., Kokko, J. (2012). "The performance of a high solar fraction seasonal storage district heating system - Five years of operation." Energy Procedia. 30, 856-865.

Smits, K.M., Cihan, A., Sakaki, S., and Illangasekare, T.H. (2011). "Evaporation from soils under thermal boundary conditions: Experimental and modeling investigation to compare equilibrium- and nonequilibrium-based approaches." Water Resources Research. 47, W05540, doi:10.1029/2010WR009533.

Thomas, H.R. and Sansom, M.R. (1995). "Fully coupled heat, moisture, and air transfer in an unsaturated soil." J Eng Mech 1995;12(3):392–405.

Thomas, H.R. and Rees, S.W. (2009). "Measured and simulated heat transfer to foundation soils." Géotechnique. 59(4), 365–375.

van Genuchten, M.T. (1980). "A closed-form equation for predicting the hydraulic conductivity of unsaturated soils." Soil Sci. Soc. Am. J. 44(5), 892–898.

Wayllace, A. and Lu, N. (2012). "A transient water release and imbibitions method for rapidly measuring wetting and drying soil water retention and hydraulic conductivity functions." Geotechnical Testing Journal. 35(1), 103-117.

Welsch, B., Rühaak, W., Schulte, D.O., Bär, K., Homuth, S., and Sass, I. (2015). "Comparative study of medium deep borehole thermal energy storage systems using numerical modelling." Proc. World Geothermal Congress 2015. International Geothermal Association. Bochum. 1-6.

Whitaker, S. (1977). "Simultaneous heat, mass and momentum transfer in porous media: A theory of drying porous media." Adv. Heat Transf. 13, 119–203.

TABLE 1. Equations used in the numerical analyses

Equation	Number	Reference
Nonisothermal liquid flow governing equation: $nS_{rw}\frac{\partial \rho_w}{\partial t} + n\rho_w \frac{dS_{rw}}{dP_c}\frac{\partial P_c}{\partial t} + \nabla \cdot \left[\rho_w\left(-\frac{k_{rw}\kappa}{\mu_w}\right)\nabla\left(P_w + \rho_w gz\right)\right] = -R_{gw}$ n=porosity (m^3/m^3), S_{rw}=degree of water saturation (m^3/m^3), ρ_w=temperature-dependent density of water (kg/m^3) (Hillel 1980), t=time(s), $P_c=P_w-P_g$=capillary pressure (Pa), P_w=pore water pressure (Pa), P_g=pore gas pressure (Pa), k_{rw}=relative permeability function for water (m/s); κ=intrinsic permeability (m^2); μ_w=temperature-dependent water dynamic viscosity (kg/(ms)) (Lide 2001), g=acceleration due to gravity (m/s^2) R_{gw}=Phase change rate (kg/m^3s)	(1)	(Bear 1972; Moradi et al. 2016)
Nonisothermal gas flow governing equation: $nS_{rg}\frac{\partial \rho_g}{\partial t} + n\rho_g \frac{dS_{rg}}{dP_c}\frac{\partial P_c}{\partial t} + \nabla \cdot \left[\rho_g\left(-\frac{k_{rg}\kappa}{\mu_g}\right)\nabla\left(P_g + \rho_g gz\right)\right] = R_{gw}$ S_{rg}=degree of gas saturation (m^3/m^3), ρ_g=temperature-dependent density of gas (kg/m^3) (Smits et al. 2011), k_{rg}=relative permeability function for gas (m/s); μ_g=temperature-dependent gas dynamic viscosity (kg/(ms))	(2)	(Bear 1972; Moradi et al. 2016)
Water vapor mass balance equation: $n\frac{\partial\left(\rho_g S_{rg} w_v\right)}{\partial t} + \nabla \cdot \left(\rho_g u_g w_v - D_e \rho_g \nabla w_v\right) = R_{gw}$ $D_e=D_v\tau$=effective diffusion coefficient (m^2/s), D_v=diffusion coefficient of water vapor in air (m^2/s) (Campbell 1985), w_v=mass fraction of water vapor in the gas phase (kg/kg), $\tau=n^{1/3}S_{rg}^{7/3}\eta$=tortuosity (Millington and Quirk 1961)	(3)	(Smits et al. 2011)
Enhancement factor for vapor diffusion, η: $\eta = a + 3S_{rw} - (a-1)\exp\left\{-\left[\left(1+\frac{2.6}{\sqrt{f_c}}\right)S_{rw}\right]^3\right\}$ a=empirical fitting parameter representing the soil-specific enhancement in vapor diffusion, f_c= clay content	(4)	(Cass et al. 1984)
Nonequilibrium phase change rate, R_{gw}: $R_{gw} = \left(\frac{bS_{rw}RT}{M_w}\right)\left(\rho_{veq} - \rho_v\right)$ b=empirical fitting parameter representing the soil-specific nonequlibrium phase change rate (s/m^2), R=universal gas constant (J/molK), ρ_{veq}=equilibrium vapor density (kg/m^3) (Campbell 1985), T=Temperature (K), ρ_v=vapor density (kg/m^3), M_w=molecular weight of water (kg/mol)	(5)	(Bixler 1985; Moradi et al. 2016)
Heat transfer energy balance: $(\rho C_p)\frac{\partial T}{\partial t} + \nabla.\left((\rho_w C_{pw})u_w T + (\rho_g C_{pg})u_g T - (\lambda \nabla T)\right) = -LR_{gw} + Q$ ρ=total density of soil (kg/m^3), C_p=specific heat of soil (J/kgK), C_{pw}=specific heat capacity of water (J/kgK), C_{pg}=specific heat capacity of gas (J/kgK), λ=thermal conductivity (W/mK), L=latent heat due to phase change (J/kg), u_w=water velocity (m/s), u_g=gas velocity (m/s), Q=heat source (W/m^3)	(6)	(Whitaker 1977; Moradi et al. 2016)

TABLE 2. Constitutive models used in the numerical analyses

Equation	**Number**	**Reference**
Soil Water Retention Curve (SWRC): $$S_{rw} = S_{rw,res} + \left(1 - S_{rw,res}\right)\left[\frac{1}{1+\left(\alpha_{vG} P_c(T)\right)^{N_{vG}}}\right]^{1-1/N_{vG}}$$ where $S_{rw,res}$ is the residual degree of saturation to water, α_{vG} and NvG are parameters representing the air entry pressure and the pore size distribution, respectively, and Pc(T) is the temperature-corrected capillary pressure according to the model of Grant and Salehzadeh (1996)	(7)	(van Genuchten 1980)
Hydraulic Conductivity Function (HCF): $$k_{rw} = \sqrt{\left(\frac{S_{rw} - S_{rw,res}}{1 - S_{rw,res}}\right)}\left[1 - \left(1 - \left(\frac{S_{rw} - S_{rw,res}}{1 - S_{rw,res}}\right)^{1/(1-1/N_{vG})}\right)^{1-1/N_{vG}}\right]^2$$ where α_{vG} and NvG are the same parameters as in Equation (7)	(8)	(van Genuchten 1980; Mualem 1970)
Thermal Conductivity Function (TCF): $$\frac{\lambda - \lambda_{\text{dry}}}{\lambda_{\text{sat}} - \lambda_{\text{dry}}} = 1 - \left[1 + \left(\frac{S_e}{S_{\text{f}}}\right)^m\right]^{1/m-1}$$ where λ_{dry} and λ_{sat} are the thermal conductivities of dry and saturated soil specimens, respectively, S_e is the effective saturation, S_f is the effective saturation at which the funicular regime is onset, and m is defined as the pore fluid network connectivity parameter for thermal conductivity	(9)	(Lu and Dong 2015)
Volumetric Heat Capacity Function (VHCF): $$\frac{C_v - C_{v\text{dry}}}{C_{v\text{sat}} - C_{v\text{dry}}} = 1 - \left[1 + \left(\frac{S_e}{S_{\text{f}}}\right)^m\right]^{1/m-1}$$ where C_{vdry} and C_{vsat} are the volumetric heat capacities of dry and saturated soil, respectively, and are similarly treated as fitting parameters, and S_f and *m* are the same parameters as in Equation (9)	(10)	(Baser et al. 2016b)

LIST OF FIGURE CAPTIONS

FIG. 12. Predicted and measured temperature time series from thermistor string T-2 for different depths (z): (a) 16.00m; (b) 14.78m; (c) 12.95m; (d) 9.29m; (e) 6.85m; (f) 1.82m

FIG. 13. Predicted and measured temperature time series from thermistor string T-3 for different depths (z): (a) 16.00 m; (b) 14.78 m; (c) 12.95 m; (d) 9.29 m; (e) 6.85 m; (f) 1.82 m

FIG. 14. Predicted and measured temperature time series from thermistor string T-4 for different depths (z): (a) 16.00 m; (b) 14.78 m; (c) 12.95 m; (d) 9.29 m; (e) 6.85 m; (f) 1.82 m

FIG. 15. Radial temperature profiles at different depths (z): (a) At the end of heating; (b) After 5 months of ambient cooling

FIG. 16. Temperature profiles along the borehole length: (a) Borehole 2; (b) Borehole 4

FIG. 17. Time series of predicted degrees of saturation at the radial locations of: (a) Borehole 3; (b) Borehole 2

FIG. 18. Radial profiles of predicted values at the end of heating: (a) Degree of saturation; (b) Thermal conductivity; (c) Volumetric heat capacity

FIG. 19. Comparison of the transient temperature response of the subsurface having thermo-hydraulic properties representative of saturated and unsaturated conditions

TRANSIENT EVALUATION OF A SOIL-BOREHOLE THERMAL ENERGY STORAGE SYSTEM

by Tuğçe Başer, Ph.D.[1] and John S. McCartney, Ph.D., P.E.[2]

ABSTRACT: This study focuses on the simulation of transient ground temperatures in a field-scale soil-borehole thermal energy storage (SBTES) system in San Diego, California. The SBTES system consists of an array of thirteen 15 m-deep borehole heat exchangers installed in conglomerate bedrock at a spacing of approximately 1.5 m. Heat collected from solar thermal panels was injected into the SBTES system over a 4-month period, after which the subsurface was monitored during a 5-month ambient cooling period. The SBTES system is located in the vadose zone above the water table with relatively dry subsurface conditions, so a coupled heat transfer and water flow model was used to simulate the ground response using thermo-hydraulic constitutive relationships and parameters governing vapor diffusion and water phase change calibrated using soil collected from the site. The simulated ground temperatures from the model match well with measurements from thermistors installed at different radial locations and depths in the SBTES system and are greater than those simulated using a conduction-only model for saturated conditions. Significant overlap between the effects of the borehole heat exchangers was observed in terms of the ground temperature. Although the numerical simulations indicate that permanent decreases in degree of saturation and thermal conductivity occurred at the borehole heat exchanger locations, the zone of influence of these changes was relatively small for the particular site conditions.

KEYWORDS: Thermal energy storage; Field-scale testing; Vertical boreholes; Unsaturated soil

---

[1] Assistant Professor, University of Illinois at Urbana-Champaign, Department of Civil and Environmental Engineering, 205 N. Mathews, Urbana, IL 61801; e-mail: tbaser@illinois.edu.
[2] Professor and Department Chair, University of California San Diego, Dept. of Structural Engineering. 9500 Gilman Dr., La Jolla, CA 92093-0085, mccartney@ucsd.edu.

1. INTRODUCTION

Soil-borehole thermal energy storage (SBTES) systems are used for storing heat collected from renewable sources in the subsurface so that it can be used later for space or water heating. Heat sources such as solar thermal panels generate heat during the day with a greater energy generation during summer months, so SBTES systems permit storage of the abundant and free thermal resource (Sibbitt et al. 2012, McCartney et al. 2013). SBTES systems function similarly to geothermal heat exchange systems, where a carrier fluid is circulated through a closed-loop pipe network installed in vertical boreholes backfilled with sand-bentonite. Different from boreholes in conventional geothermal heat exchange systems, the boreholes in SBTES systems are spaced relatively close together (1-2 m) in an array to concentrate heat in the subsurface (Claesson and Hellström 1981). SBTES systems are a convenient alternative to other energy storage systems as they are relatively inexpensive, involve storage of renewable energy (solar thermal energy), and are space efficient as they are underground (Başer and McCartney 2015a).

Despite the successful use of SBTES systems in community-scale applications (Sibbitt et al. 2012; Nussbicker-Lux 2012; Bjoern 2013), there are still opportunities for engineers to improve the performance of SBTES systems by considering the role of the hydrogeological setting in the subsurface. A goal of this study is to understand the benefits of installing SBTES systems in the vadose zone, the layer of unsaturated soil or rock near the ground surface that may extend to depths greater than 10 meters in some locations. The unsaturated porous material in the vadose zone has a lower thermal conductivity than when saturated, limiting the transient spreading of heat away the subsurface heat storage system (Choi et al. 2011). The volumetric heat capacity of soils in unsaturated conditions is lower than in saturated conditions but is still greater than in dry conditions. For example, the volumetric heat capacity of a silty soil is 2.5 MJ/m^3K for saturated conditions, 2.0 MJ/m^3K for a degree of saturation of 0.5, and 1.2 MJ/m^3K for dry conditions (Baser et al. 2016d). One challenge is that the modes of heat transfer in unsaturated porous materials are more complex than when dry or water-saturated. Specifically, in addition to coupling between the thermal and hydraulic properties of unsaturated soils and the effects of temperature on fluid properties (e.g., Lu and Dong 2015), the modes of heat transfer in unsaturated soils include a combination of conduction, convection due to the flow of pore water in liquid and vapor forms under thermal and hydraulic gradients, and latent heat transfer due to phase change. Several studies have developed models to capture these different mechanisms of coupled heat transfer and water flow in unsaturated soils, and have applied them to problems associated with radioactive waste repositories (e.g., Ewen and Thomas 1989; Thomas and Sansom 1995; Gens et al. 1998; Gens et al. 2009), soil-atmosphere interaction (Smits et al. 2011), energy piles (Akrouch et al. 2016), and borehole geothermal heat exchangers (Başer et al. 2018). Başer et al. (2018) found that the zone of influence of temperature changes in silt around a heat exchanger were greater for unsaturated conditions when considering the impact of vapor phase convection. Previous simulations of geothermal heat exchangers in unsaturated soil used conduction alone with a thermal conductivity that varies with the initial degree of saturation (e.g., Choi et al. 2011), but Başer et al. (2018) found that thermally-induced water flow may lead to significant differences in the thermo-hydraulic response of the subsurface.

This paper presents a comparison of transient changes in ground temperatures measured in a field-scale SBTES system installed in the vadose zone in San Diego, California with those predicted from a numerical model for coupled heat transfer and water flow. The testing program involved a 4-month period where heat collected from solar thermal panels was injected into the borehole array, followed by a 5-month ambient cooling period. Heat transfer rates into the subsurface measured in the field-scale SBTES system were used to define the dynamic boundary conditions for heat injection in the model, considering the effects of fluctuations in surface air temperature. Although the primary variable from the comparison is the ground temperature, the numerical model also permits evaluation of the effects of thermo-hydraulic interaction between the closely-spaced boreholes in the SBTES system on the degree of saturation. This is important as changes in the degree of saturation due to thermally-induced water flow may lead to associated changes in the subsurface thermo-hydraulic properties of unsaturated soils.

2. BACKGROUND

Since the concept of borehole thermal energy storage systems was introduced by Claesson and Hellström (1981), several SBTES systems have been installed in Canada and Europe as part of district-scale heat distribution systems. The Drake Landing SBTES system in Okotoks, Alberta, Canada supplies heat from solar thermal panels installed on garage roofs to an array of 144 boreholes in a 35 m-deep, 35-m wide grid (Sibbitt et al. 2012), which is then used to supply approximately 90% of the heat demand of 52 homes. Catolico et al. (2016) simulated the response of the Drake Landing SBTES system, which lies in water-saturated sand deposits overlying glacial till, using a numerical model in TOUGH2 using time-dependent injection fluid temperatures measured at the site over six years of operation as the main boundary condition. Over each year of operation, lateral heat transfer from the borehole array to the surrounding ground was found to decrease due to a reduction in the thermal gradient between the center of the array and the surrounding subsurface, meaning that more thermal energy was concentrated in the center of the array. They found that the annual efficiency of heat extraction (heat extracted divided by heat injected) increases over time, approaching a value of 55%. However, the efficiency of heat recovery was found not to be a good quantification of the SBTES performance because if the demand for heat in a given winter is lower the the efficiency will decrease. Instead, it may be better to evaluate the fractions of heat injected, stored, and lost. For example, in the 6th year of operation, 31.5% of the heat injected into the system was recovered, 21.9% of the heat injected remained in the borehole array, and 46.7% of the heat injected escaped the borehole array. Despite the seemingly high fraction of heat loss, the heat stored and recovered was sufficient to provide more than 90% of the community's annual heating demands. Another successful SBTES system was installed in 2007 is in Braedstrup, Denmark (Bjoern 2013). This system supplies heat from 18,000 m^2 of solar thermal panels to an array of 50 boreholes having a depth of 47 to 50 m installed across a 15 m-wide area. This system provides 20% of the heat to 14,000 homes. Another commercial-scale SBTES was installed in 2008 in Crailsheim, Germany involving of a series of 55 m-deep boreholes that formed a 39,000 m^3 subsurface storage volume. This system stores heat from 7410 m^2 of flat plate solar thermal collectors to provide heat for a school and 230 dwellings (Nussbicker-Lux 2012).

Although the experience from the commercial-scale systems at Drake Landing, Braedstrup and Crailsheim indicates that SBTES systems are functional and are sufficiently efficient to provide heating to different sizes of communities, simulation studies such as that of Catolico et al. (2016) indicate that the hydrogeological setting is critical for optimizing the thermal energy storage. Although the Drake Landing SBTES system includes instrumentation to evaluate changes in ground temperature within the array (Sibbitt et al. 2012), it is in use for commercial purposes, so the heat injection patterns cannot be varied as part of scientific studies on the performance of SBTES systems. Accordingly, it is advantageous to install smaller SBTES systems for demonstration projects in different hydrogeological settings to understand the roles of different heat transfer processes and heat injection patterns on SBTES system performance. For example, Başer et al. (2016a) reported the ground temperatures monitored during a 75-day heat injection experiment into a small-scale SBTES system in Golden, CO, USA involving an array of 5 borehole heat exchangers. Although the SBTES system in that study was installed in an unsaturated silty soil layer, observations during installation indicate that the bottom 10% of the heat exchanger lengths were in a saturated sand aquifer underlying the site. Transient temperature measurements indicated that a substantial portion of the injected heat left the array due to lateral heat loss associated with both the higher thermal conductivity of the saturated sand layer and possible convection effects associated with groundwater flow in this sand layer. Further, the simulations of Başer and McCartney (2015b) indicate that arrays should have a greater number of boreholes than those considered by Başer et al. (2016a) to effectively concentrate heat in the subsurface.

Although simplified design models for SBTES systems have been developed (e.g., Claesson and Hellström 1981), modeling the transient heat transfer in SBTES systems can be complex because of the dimensions of the problem, the geometry and structure of the borehole network, the process of heat transfer into the ground via circulating fluids in closed-loop pipe networks, and the nonlinear variations in the thermal and hydraulic properties of unsaturated soils with degree of saturation. Marcotte and Pasquier (2014) investigated the effect of the borehole arrangement both analytically and numerically on the thermal response of a heat storage system for the cases in which boreholes are connected in series, parallel, and mixed configurations. They reported significantly lower inlet fluid temperatures for the parallel configuration than for the series configuration, indicating a larger heat transfer to the ground for this arrangement compared to the series configuration. Besides the geometrical configuration of the borehole heat exchangers and the fluid circulation configuration (series, parallel, mixed), there are other factors that affect the thermal response of a storage system, such as the subsurface temperature profile and ambient air temperature, degree of saturation profile of soil and the thermal properties. Thomas and Rees (2009) investigated the effect of water content on heat transfer through unsaturated soils via a series of one and two-dimensional numerical simulations that consider only conduction as the major heat transfer mechanism. They reported 60% and 20% increases in heat flux with increasing water content for one- and two-dimensional models, respectively. Akrouch et al. (2016) proposed an analytical solution based on cylindrical heat source theory that accounts for variable degree of saturation on the heat exchange between the heat source and sand soil and the results indicated a 40% drop in performance of a heat exchanger when the degree of saturation is close to residual conditions. Welsch et al. (2015) studied the impact of borehole length, borehole, spacing, number of boreholes, and the inlet heat transfer fluid temperatures on the behavior of thermal energy storage in crystalline rock. They observed that there was an optimal spacing to reach the highest efficiency of heat recovery, with higher and lower values leading to lower efficiencies. Due to the high thermal conductivity of the crystalline rock, the optimal borehole heat exchanger spacing was 5 m, which is greater than that observed in similar studies the focus on lower thermal conductivity soils (e.g., Baser and McCartney 2015a). Welsch et al. (2015) found that the number of boreholes has a positive influence on the efficiency of heat recovery because the increasing ratio of the storage volume to the size of the boundary of the storage volume results in lower heat losses to the surrounding subsurface outside of the array.

Başer and McCartney (2015a) used a conduction-only model to understand the impacts of borehole array geometry, ground properties, heat injection magnitudes, and heat injection duration on the temperature distribution in the SBTES system. Başer et al. (2016b) and Başer et al. (2016c) used a coupled heat transfer and water flow model without considering vapor diffusion or phase change to understand the roles of incorporating a thermal insulation layer and the effect of different unsaturated soil properties on the ground temperatures in SBTES systems, respectively. These studies found that a surface insulation layer does not play a significant role on the thermal energy storage due to the small area around each borehole heat exchanger, but that surface temperature fluctuations should still be considered on the ground temperatures. Bidarmaghz et al. (2016) investigated the effect of surface air temperature changes on the thermal response of geothermal heat exchangers in the shallow subsurface and found that considering ambient air temperatures in the simulations increased the total heat exchanger length by 11%. A similar study by Nguyen et al. (2017) showed that seasonal temperature variation of the subsurface increases the outlet fluid temperature causing a decrease in the heat transfer rate into the ground. Further, they found that burying boreholes at the certain depth from the surface (1-2 m) is not sufficient to hinder the ambient air temperature effects on the ground temperature near the surface. Baser et al. (2017) used a coupled heat transfer and water flow model considering vapor diffusion and phase change to study the response of a single vertical borehole heat exchanger during a heat injection period followed by a, ambient cooling periods. They evaluated the role of different heat transfer mechanisms and observed a permanent drying around the heat exchanger during heat injection that was not recovered during ambient cooling. This drying led to a decrease in thermal conductivity that corresponded to a reduction in the amount of heat loss from the soil near the heat exchanger.

3. NUMERICAL MODEL

3.1. Model Formulation

This study applies the model for geothermal heat exchangers in unsaturated soils used by Baser et al. (2018), which was originally developed by Smits et al. (2011) and enhanced by Moradi et al. (2016), to simulate the behavior of a field-scale SBTES system installed in San Diego, California. The governing equations for the model are summarized in Table 1, while the key thermo-hydraulic constitutive relationships are summarized in Table 2. Coupling occurs between the different equations in Table 1 due to the effects of temperature on the different fluid properties, which are summarized by Smits et al. (2011) and Baser et al. (2018). Simulation of coupled heat transfer and water flow in unsaturated soils requires simultaneous solution of the governing equations for two-phase flow (Equations 1 and 2) along with the heat transfer based on energy balance (Equation 6). Because liquid and vapor phases are present in unsaturated soils, flow induced by thermal gradients in both liquid and total gas phases are considered and formulated as the convection terms in the energy balance equation (i.e., the second and the third terms in Equation 6). When formulating the model, some assumptions are made: (a) soil framework is homogeneous, isotropic, and non-deformable; (b) fluid phases are immiscible; (c) hysteresis in the constitutive relationships is not considered. The model considers enhanced vapor diffusion described by Equation (4) and a nonequilibrium phase change rate described by Equation (5) that are incorporated into the water vapor mass balance equation in Equation (3) and as source terms in the governing equations for two-phase flow and the heat transfer energy balance. The model was implemented into the finite element-based software COMSOL Multiphysics® version 5.2a (COMSOL 2015) which solved the governing equations for the four primary unknowns: pore water pressure, total pore gas pressure, water vapor concentration, and temperature.

3.2. Model Calibration

The key parameters that must be defined to calibrate the numerical model are the parameters of the thermo-hydraulic constitutive relationships given in Table 2 and the parameters *a* and *b* from Table 1 that govern the soil-specific enhanced vapor diffusion rate and the nonequilibrium phase change rate, respectively. The methodology described in this section for parameter calibration was applied to the subsurface in the SBTES array evaluated in this study but could also be applied to design SBTES systems in the vadose zone in other locations.

The SBTES system constructed as part of this study was installed in an unsaturated conglomerate bedrock layer at the Englekirk Structural Engineering Center (ESEC) of the University of California San Diego. A site investigation from 2003 indicates approximately 1m of sandy soil overlying the conglomerate bedrock consisting of cemented sand- and gravel-size particles. An undisturbed core of the conglomerate bedrock was not obtained during installation of the SBTES system. However, disturbed cuttings from a hole drilled into the conglomerate using an auger were collected from different depths. Although it is not possible to reconstitute the cuttings into the same cemented structure as the conglomerate, it is assumed that the thermo-hydraulic properties of the conglomerate are predominantly governed by the grain size, mineralogy, and density for the purposes of model calibration so that laboratory calibration of the model parameters is possible. Laboratory calibration permits the use of instrumented specimens under carefully-controlled boundary conditions, but future studies may use inverse analyses from field measurements to consider the role of the cemented structure on the calibrated model parameters. Specimens used to represent the conglomerate properties were reconstituted from cuttings obtained from a depth of 16 m from the surface at the ESEC facility, which were prepared using compaction to a dry density of a 1650 kg/m^3 at an initial degree of saturation of 0.49, which corresponds to conditions in the conglomerate measured using sand-cone experiments performed at a depth of 1.5 m from the surface.

The thermo-hydraulic constitutive relationships were determined using a modified form of the transient water release and imbibition method (TRIM) of Wayllace and Lu (2012) that included the measurement of the thermal conductivity and volumetric specific heat capacity described by Lu and Dong (2015). Specifically, a specimen was compacted to the conditions mentioned above into a modified Tempe cell that incorporates a dual thermal needle and a dielectric sensor, was saturated with water, then dried monotonically in two stages. The soil water retention curve (SWRC), hydraulic conductivity function (HCF), thermal conductivity function (TCF), and volumetric heat capacity function (VHCF), described by Equations 7 through 10 in Table 2, were obtained from inverse analysis of the outflow and thermal property measurements during this drying stage. The SWRC and HCF along with relevant parameters are shown in Figure 1(a), while the TCF and VHCF along with relevant parameters are shown in Figure 1(b). Lu and Dong (2015) presented empirical relationships between the parameters of the thermal constitutive relationships and the hydraulic constitutive relationships, but the properties measured from the experiments in Figure 1 were used in the simulations.

The properties governing the vapor diffusion phase change rate and diffusion were calibrated using an evaporation experiment on a reconstituted specimen of the site soil. The soil was compacted in a plastic modified Proctor compaction mold having a diameter of 152 mm to a height of 179 mm. The mold, developed by Iezzoni and McCartney (2015), can accommodate a dielectric sensor at mid-height of the soil specimen as shown in the cross-sectional schematic in Figure 2. An evaporation test starting from the initial degree of saturation mentioned above was performed by heating the bottom of the soil layer using a heating pad placed below the mold while leaving the surface of the soil open to the atmosphere. The heating pad applies fluctuating heat pulses to maintain a target temperature. Thus, a thermocouple was placed at the bottom to monitor the applied boundary temperature during heating, which is shown in Figure 3(a). Ambient temperatures were also recorded with a thermocouple so that the ambient air temperatures could be applied as boundary conditions on the outer surfaces of the specimen during the experiment. A temperature of approximately 42 °C was maintained over a period of 35 h. The measured values of temperature and degree of saturation at the center of the soil specimen during this period are shown in Figures 3(a) and 3(b), respectively. The model of Iezzoni and McCartney (2015) was used to correct the degrees of saturation inferred from the dielectric sensor to account for temperature effects. This calibration test was then simulated using the coupled heat transfer and water flow model, and the parameters *a* and *b* in Equations 4 and 5 in Table 1 were varied using a manual parameter sweep to identify the best combination of parameters to match the measured curves. The simulated temperature and degree of saturation curves for $a = 20$ and $b = 2\times10^{-7}$ s/m^2 are shown in Figures 3(a) and 3(b), respectively, which indicate a good match.

3.3. Simulation Details for the Field-Scale SBTES System

The calibrated model was then used to simulate the response from the field-scale SBTES system demonstration experiment. A plan view of the SBTES system showing the connections between the boreholes in the array, a manifold for control and monitoring of the heat exchanger fluid in the borehole array, a 2400 L water-filled temporary heat storage tank, and a series of solar thermal panels is shown in Figure 4(a). This figure also shows the location a reference borehole for monitoring the undisturbed ground temperature profile. Thirteen of the boreholes in the array include heat exchanger tubing, while four of the boreholes in the array include thermistor strings that monitor the ground temperature. Two of the boreholes include both heat exchangers and thermistor strings. The boreholes were backfilled with sand bentonite after installation of the heat exchangers or thermistor strings. The hexagonal configuration of the borehole array was selected for ease of construction, as the boreholes in the array fall into five co-linear sets that facilitate positioning of the drill rig. The main design variable used to configure the boreholes was the spacing. Baser and McCartney (2015a) found that the borehole spacings should be less than 1.5 m to ensure overlapping effects of the heat exchangers for soil thermal properties and heat transfer rates typical of SBTES systems. The number of boreholes containing heat exchangers was selected so that the boreholes in the array would fall into two annuli, greater than the number in the array tested by Baser et al. (2016a). Although a commercial-scale SBTES system would likely have more heat exchangers in several more annuli (e.g., Sibbitt et al. 2012), this array is still sufficient in scale to investigate the transient heat transfer and heat storage in the subsurface within the array associated with interactions between heat exchangers.

An elevation view of the site is shown in Figure 4(b), which highlights the position of the 15 m-long boreholes beneath a 1 m-deep excavation. After connection of the heat exchanger tubing following the arrangement shown in Figure 4(a), a thin layer of site soil was placed for leveling-purposes, which was overlain by a hydraulic barrier, an insulation layer, and a compacted layer of site soil. The high-density polyethylene (HDPE) hydraulic barrier has a thickness of 0.01 m and an assumed hydraulic conductivity of 10^{-12} m/s, while the EPS geofoam insulation layer has a thickness of 50 mm, a thermal conductivity of 0.03 W/mK, and a specific heat capacity of 0.9 MJ/kgK. The lateral extents of the hydraulic barrier and insulation layer followed the hexagonal boundaries of the array shown in Figure 4(a). Pictures of the SBTES system are shown in Figure 5, highlighting the 1 m-deep excavation and connection of the borehole heat exchangers in Figure 5(a), the hydraulic barrier in Figure 5(b), the insulation layer in Figure 5(c), and the completed set of solar thermal panels and temporary heat storage tank in Figure 5(d).

As the hexagonal borehole array is symmetrical, a quarter section was simulated as shown in Figure 6. The temperatures on either side of the two planes of symmetry are assumed to be identical. This simulation strategy was also used by Catolico et al. (2016) to reduce computation times when simulating symmetrical SBTES systems. Figure 6 also includes the labels used to name the thirteen boreholes that include heat exchangers (boreholes A through M) and the four boreholes that include thermistor strings (T-1 to T-4). As will be described below, appropriate fractions of the heat transfer from boreholes A (1/4 of its heat transfer), B (1/2 of its heat transfer) and E (1/2 of its heat transfer) are applied as boundary conditions. The model domain is 15 m x 15 m in plan and has a depth of 20 m and includes 5 borehole heat exchangers. The size of the domain was selected such that the heat exchangers would not affect the temperatures at the boundaries for the heat injection period under investigation. This was confirmed by ensuring that the temperature at the boundaries of the array remained similar to the temperatures from the reference borehole at different depths. The domain was discretized using 756,667 elements with finer discretization around the boreholes. Triangular elements were used on the surfaces of boreholes and insulation layer, and tetrahedral elements were used for the rest of the domain. A maximum element growth rate of 1.4 and a curvature factor of 0.25 were used in discretization in COMSOL.

The isometric views of the model domain shown in Figures 7(a) and 7(b) highlight the thermal and hydraulic boundary and initial conditions, respectively. The initial temperature profile was obtained from the ground temperature distribution measured by the reference borehole at the initiation of the heat injection period on April 29th, 2016. To define the initial degree of saturation profile, hydrostatic conditions were assumed. Although the water table was not encountered in the previous geotechnical site investigation which was performed in 2003, the San Diego County Water Authority reported that the ground water depth ranges in depth from 14 to 24 m in the area and no groundwater flow was recorded. Accordingly, the water table was fixed at a depth of 20 m from the surface (i.e., at the base of the domain) throughout the simulations for simplicity as its actual location during the experiment is unknown. Although the depth of the groundwater table may be greater than 20 m, this choice of boundary condition was selected to limit the size of the domain in the simulations. Based on the hydrostatic profile shown in Figure 7(b), the initial degree of saturation along most of the length of the heat exchangers was approximately 0.22 which corresponds to residual saturation conditions. Near the bottom of the heat exchangers, the initial degree of saturation increases up to 0.49 due to the proximity of the water table.

Neumann boundary conditions of zero mass flux and zero heat flux were assigned for the outer lateral boundaries of the domain as well as for the planes of symmetry. Dirichlet boundary conditions for temperature were applied at the bottom and top of the domain. A constant temperature of 21°C was applied at the bottom of the domain, which corresponds to the average measured temperature at the base of the reference borehole. The temperature of the top of the domain was assumed to equal the time-dependent ambient air temperatures that were measured at the site during the duration of the experiment, shown in Figure 8(a). Although the EPS geofoam insulation layer is considered in the simulations, it does not provide a perfect insulation effect so the effects of the ambient air temperature fluctuations on the surface temperature must be considered. It should be noted that the surface ground temperature may differ from the ambient air temperature due to radiative and air convection effects, so the use of the ambient air temperature as a surface boundary condition may be a simplifying assumption. A zero-mass flux boundary condition was applied to the surface boundary. This choice was made to simplify the fluid flow processes in the ground as an infiltration/evaporation boundary condition can be computationally expensive when combined with a coupled heat transfer and water flow model considering vapor diffusion and phase change. However, this assumption is reasonable both due to the relatively low precipitation in San Diego as well as due to the presence of the hydraulic barrier atop the borehole array. However, this boundary condition choice is expected to affect the accurate simulation of the temperature at the location of the reference borehole, as infiltration of water may affect the thermal properties of the surface soil. As mentioned, Dirichlet boundary conditions were assumed for the water table at the base of the domain (pore water pressure equal to zero).

Although the heat transfer boundary conditions for geothermal borehole heat exchangers previous simulations of SBTES systems involved control of the inlet fluid temperature and considered convective heat transfer associated with fluid flow through the sequence of borehole heat exchangers in the array (e.g., Welsch et al. 2015; Catolico et al. 2016), this study considered the borehole heat exchangers as cylindrical heat sources and applied heat flux values to the outer diameters of the cylinders equal to the measured heat flux values from the site discussed in the next paragraph. The heat transfer boundary conditions associated with fluid flow through heat exchanger pipes were not considered in this study because of long computational times associated with solving the governing equations for coupled heat transfer and water flow processes in the subsurface given in Table 1, which was the primary topic of interest in this study. The simplified heat transfer boundary condition for the borehole heat exchangers still permits validation of the coupled heat transfer and water flow analyses in the subsurface within the array. However, design simulations for SBTES systems require control of the inlet fluid temperature and consideration of convective heat transfer of fluid flow through the heat exchangers as the heat transfer rate will decrease over time as the soil within the array increases in temperature (e.g., Welsch et al. 2015). Another assumption in this study is that a uniform heat flux was applied to each of the heat exchangers based on the measured heat transfer rates in the field. Although the choice of a uniform heat flux along a heat exchanger connected in series through several boreholes may not be suitable when simulating a commercial-scale SBTES system with long overall heat exchanger lengths, the relatively short overall heat exchanger lengths used in this field demonstration project permitted the use of this simplified boundary condition without major discrepancies in matching the measured subsurface temperatures.

Eight evacuated tube solar thermal panels having a total area of 33 m^2 were connected in series to collect heat during the day, which was then transferred to the water in the temporary heat storage tank via a coiled copper tube. A second coiled copper tube in the temporary heat storage tank is used to inject heat into the SBTES system. A second horizontal SBTES system was also installed at the site and was tested at the same time (Baser et al. 2019). Although this horizontal SBTES system is not discussed in this paper, it should be acknowledged as all the heat collected from the solar thermal panels was not injected into the “vertical” SBTES system under evaluation in this study. Nonetheless, the measured heat transfer rate into the subsurface was boundary condition used in the simulations, so the effects of the horizontal SBTES system is not important. Water was used as the heat exchanger fluid in both the solar thermal panels and in the SBTES system as freezing temperatures are not expected in San Diego. The heat transfer rates were calculated as follows:

$$\dot{Q} = \dot{V}_w \rho_w C_w \left(T_{in} - T_{out}\right) \tag{11}$$

where $\dot{V}_w$ is the measured volumetric flow rate of the heat exchanger fluid (water), ρ_w is the density of water (1000 kg/m^3), C_w is the specific heat capacity of water (4183 J/kgK), and T_{in} and T_{out} are the measured temperatures of the water entering and exiting solar thermal panels, respectively. The heat transfer rates for the solar thermal panels over the 120-day period starting on April 29, 2016 are shown in Figure 8(b). The large fluctuations in heat transfer rate observed in this figure occur because heat is only collected during the day. To better understand the transient heat transfer rates from the solar thermal panels and the total heat injected into the vertical SBTES system during 2 days of operation are shown in Figure 8(c). A lag is observed between the heat transfer rates collected from the solar thermal panels and injected into the vertical SBTES, but the temporary water storage tank provides a buffer to permit heat injection at night as well. A control system has not yet been implemented to ensure that heat is only collected from the solar thermal panels during the day. Specifically, the circulation pumps in the solar thermal panels and SBTES system are operated continuously. Accordingly, fluid is still circulated through the solar panels at night, which may result in a slight extraction of heat from the temporary heat storage system if the outside air is colder than the borehole array. The efficiency of heat transfer in the system can be assessed using the cumulative total energy collected from the solar thermal panels and injected into the vertical and horizontal SBTES systems shown in Figure 8(d). Approximately 80% of the cumulative heat collected from the solar thermal panels is injected into the vertical and horizontal SBTES systems, with the remaining 20% lost due to the circulation of fluid through the solar thermal panels at night. Additional experimental testing is underway to investigate other configurations for flow through the solar thermal panels (series instead of parallel) along with inclusion of a heat transfer fluid control system in the solar thermal panels to increase the efficiency of heat collection from the solar thermal panels and injection into the SBTES systems.

As mentioned, the borehole heat exchangers were simulated as cylinder sources having a uniform heat flux with depth with a magnitude that varied according to the measured heat flux interpreted from Equation (11) using the entering and exiting fluid temperatures and fluid flow rates going into the different geothermal loops shown in Figure 4(a). Specifically, the heat exchanger tubing was split into three closed-loop networks of U-tube borehole heat exchangers (referred to as Loops 1, 2, and 3). Each loop is connected to a borehole heat exchanger in the central borehole, which means that the central borehole contains 3 U-tube heat exchangers. Next, the three loops connect to four other borehole heat exchangers in different zones of the array, as shown in the photograph in Figure 9 and the schematic in Figure 4(a). It is expected that the heat exchanger fluid flowing through the loops will be hottest in the center of the array, and the fluid temperature will decrease as it flows through the surrounding four borehole heat exchangers and returns to the manifold. However, as noted above, the relatively short length of the heat exchangers in each loop permits the assumption that the heat flux is the same from each borehole connected to the loop (except for the central borehole which has three times the other boreholes). The use of three loops provides flexibility for changing the heat transfer into different zones of the array, but in this study all three loops had a balanced flow. Specifically, the fluid flow rates in each of the loops were controlled and measured independently to be equal and ensure that heat transfer is balanced into the different zones of the borehole array. The inlet and outlet fluid temperatures for each loop were monitored so that Equation (11) could be applied to obtain the heat transfer rate into the subsurface, which was the main boundary condition applied in the simulations.

A challenge encountered when simulating a quarter domain is that boreholes from different loops were included in the domain, and the heat transfer rates in each loop were not the same. Specifically, the borehole heat exchangers that were simulated were A (center borehole, part of loops 1, 2, and 3), B (part of loop 2), C (part of loop 2), and D (part of loop 3), E (part of loop 3) as shown in Figure 9 and Figure 4(a). Further, the heat transfer rates calculated using Equation 11 represent an average heat transfer rate across the five borehole heat exchangers in each loop. Accordingly, some assumptions had to be made regarding the heat transfer rates applied to the different borehole heat exchangers being simulated. Because the different borehole heat exchangers were obtained from different loops, the heat transfer rates for the different borehole heat exchangers were interpreted from the heat transfer rates of Loops 1, 2, and 3 calculated from Equation 11 which are shown in Figure 10. Specifically, the total heat transfer rates from all three loops were first divided by five to represent the heat transfer rate into the five boreholes in the quarter section domain and the transient heat fluxes were applied to each borehole individually depending on its associated loop. The heat transfer rate for the center borehole was equal to the sum of $1/5^{th}$ of each of the three heat transfer rates, and the heat transfer rates for boreholes B, C, D, and E were equal to $1/5^{th}$ of the heat transfer rates from the respective loops noted above. Although it is likely that the center borehole A had a higher local heat flux than the outer borehole E it is assumed that the gradients of temperature in the center and edge of the array balanced out over time, so the total heat transfer rate of each loop could be considered as an average of the entire system. The transient heat transfer rates were converted to heat fluxes which were applied to the outside area of each borehole in the quarter section domain. At the end of the heat injection period, the heat flux for each borehole was set to zero to represent the ambient cooling period. Because the coupled heat transfer and water flow processes in the subsurface are relatively slow, a time interval of 1800 s was used in the simulations of the 120-day heat injection period followed by a 155-day ambient cooling period, which was found to lead to sufficiently accurate results when evaluating the changes in ground temperature.

4. COMPARISON OF NUMERICAL RESULTS AND FIELD MEASUREMENTS

A goal of this study is to present the field measurements in a way that the transient heat transfer results at different locations in the borehole array could be understood. Second, because of the simplifying assumptions regarding the subsurface thermo-hydraulic properties (homogeneity and use of reconstituted specimens), the uncertain location of the water table below the heat exchanger array, and the use of a uniform heat flux along the boreholes, it is preferred to show a qualitative comparison between the field measurements and the results from the numerical simulation without a detailed error analysis.

As could be expected from the large fluctuations in the heat transfer rate into the geothermal heat exchanger loops due to the variability in the solar thermal heat transfer rate, the temperature at the locations of the borehole heat exchangers are expected to experience significant changes in temperature each day. The temperatures at the center borehole measured using the thermistor string T-1 along with the simulated temperature from the model are shown in Figure 11. The temperature at each depth is shown separately in each sub-figure to differentiate the transient response at the different depths. Although the temperatures at a depth of 16.00 m were underestimated during heating, the temperatures at other depths were captured well by the model. The difference at a depth of 16.00 m may be due to the assumption of the hydrostatic initial conditions based on the assumed location of the water table, which leads to a higher thermal conductivity of the subsurface in the simulations. The differences in the daily fluctuations of each depth occur as the temperatures from the model were obtained in a soil element at the boundary of the heat exchanger, while the measured temperatures are from the thermistor strings inside the borehole and are in contact with the geothermal heat exchanger. The sand-bentonite grout backfill in the boreholes was not considered in the model simulations but may affect the heat transfer process in the field measurements. During the ambient cooling stage, the transient trends appear to be well-captured, although the initial temperature at the start of ambient cooling was occasionally different from that between the measured and simulated values. The two locations closer to the surface show an increase in the rate of cooling on day 210, likely due to the lower ambient air temperatures observed in Figure 8(a).

A comparison between the temperatures at the location of thermistor string T-2 shown in Figure 12 indicates less daily fluctuations than at the location of thermistor string T-1. The temperature at the location of thermistor string T-2 depends on overlapping effects of borehole heat exchangers A and B, and heat transfer from these boreholes damps out the daily fluctuations. A good match in the trends and magnitudes at the different depths was observed during both the heat injection and ambient cooling periods, with underestimation of the temperatures at depths of 16.00 m and 1.82 m. The measured temperature values during the heating injection period ranged from 29.5 °C near the bottom of the array to 34.2 °C near the top of the array. The greater increases in measured and simulated temperatures near the surface of the array may be due to greater heat transfer in initially dryer soils due to greater water vapor diffusion and latent heat transfer as well as buoyancy-driven upward movement of water vapor, both of which were observed by Baser et al. (2018) in the simulation of a single geothermal heat exchanger. The measured and simulated temperatures at the location of thermistor string T-3 shown in Figure 13 are similar to those for thermistor string T-1 in Figure 11 due to the presence of borehole heat exchanger B, but with lower magnitudes. The lower magnitude is because the heat flux from borehole heat exchanger B was three times smaller than the three loops in borehole heat exchanger A. Finally, the measured and simulated temperatures at the location of thermistor string T-4 shown in Figure 14 show the lowest increases in temperature due to its larger radial location from the center of the borehole array. One of the thermistors at a depth of 12.95m was not functional after installation. Like thermistor string T-2, greater temperatures were noted near the surface.

The differences between the simulated and measured ground temperatures could be due to the use of reconstituted specimens to obtain the thermo-hydraulic properties, the possibility that the subsurface does not have homogeneous thermo-hydraulic properties, uncertainty about the actual depth of the groundwater table (which may have affected the initial degree of saturation and thermal properties), and the use of simplified heat exchanger boundary conditions. A general observation regarding the measured and simulated temperature time series is that even though the heat transfer was simulated as an average heat flux at the boundaries of the heat exchangers instead of simulating the heat transfer via circulation of fluid in the borehole loops, a good match with the ground temperatures during both heating and cooling was observed. Although the actual location of the water table was not known a-priori, comparison of the simulation results shown in Figures 11 through 14 at depths near the middle and bottom of the heat exchangers indirectly reflect the importance of the initial degree of saturation on the simulation results from the coupled heat transfer and water flow model. Greater initial degrees of saturation will lead to higher thermal conductivity values and may lead to greater changes in degree of saturation due to enhanced vapor diffusion and latent heat transfer (Baser et al. 2018). The differences in simulated and measured temperatures at the different depths in the soil profile in Figures 11 through 14 could also have been due to variations in subsurface stratigraphy not observed in the installation of the heat exchangers, which would have led to variations in thermo-hydraulic properties with depth. Despite the challenges in validating the numerical model with field data, the numerical model was found to capture the temperature of the subsurface within the array with good accuracy within most of the array.

Radial profiles of temperatures at the end of the heat injection period from the numerical model and the field measurements are shown in Figures 15(a) for the depths that thermistors were installed. Temperatures were in good agreement, especially at depths of 14.78 and 1.82 m. This figure also includes the ground temperatures from the reference borehole. The shapes of the radial profiles are like those interpreted from the field measurements, although the maximum temperatures at the locations of thermistor strings 1 and 3 due to the daily fluctuations in heat transfer rate were not captured as noted in the time series in Figures 11 and 13, respectively. Radial distributions in temperature at the end of the ambient cooling period indicate that some heat (a maximum difference in temperature of 4 °C from the initial value of 21 °C) is still retained within the array after 5 months of ambient cooling. This amount of decrease in temperature due to ambient cooling is expected to decrease if further cycles of heating and cooling were investigated, similar to the observations of Catolico et al. (2016). Temperature profiles at the locations of boreholes 2 and 4 are shown in Figures 16(a) and 16(b), respectively. Both the measured and simulated temperature profiles show an increase in temperature with proximity to the ground surface, likely due to the effects of natural convection. As the pore fluids are heated, their densities decrease causing them to rise and transfer heat upward in the subsurface.

5. ADDITIONAL INSIGHTS FROM MODEL SIMULATIONS

Although it was known that the subsurface at ESEC was unsaturated, and that changes in degree of saturation are expected due to coupled heat transfer and water flow, instrumentation was not incorporated in the subsurface within the borehole array to monitor changes in degree of saturation. This was due to difficulty in installing dielectric sensors into the intact conglomerate through the sides of the boreholes. Installation of these sensors into a soil-bentonite-backfilled borehole would measure the changes in thermo-hydraulic behavior of the backfill, not the conglomerate. Nonetheless, it is still possible to infer the changes in degree of saturation of the subsurface from the numerical simulation results, as well as the effects of these changes on the heat transfer during the heat injection period and heat retention during the ambient cooling period. Time series of the simulated degrees of saturation at the locations of thermistor strings 3 and 2 are shown in Figures 17(a) and 17(b). Due to the boundary conditions associated with borehole heat exchanger B next to thermistor string 3, a steady decrease in degree of saturation was noted during the heat injection period at this location in Figure 17(a). This decrease in degree of saturation is expected due to enhanced vapor diffusion from relatively hot regions to colder regions. During the ambient cooling stage, the degree of saturation at the location of thermistor string T-3 was not observed to recover. A similar observation was made by Baser et al. (2018) for a single borehole heat exchanger in compacted silt that had different thermo-hydraulic properties. The main effect of this decrease in degree of saturation is that the decrease in temperature at this location during ambient cooling should be slower due to the lower thermal conductivity associated with the permanent decrease in degree of saturation. An interesting observation is that this same decrease in degree of saturation during the heat injection period was not observed in Figure 17(b) at the location of thermistor string T-2, which was between borehole heat exchangers A and B. In fact, a slight increase in degree of saturation is observed, likely due to movement of water vapor away from these two heat exchangers to the cooler regions between.

The differences in behavior at the locations of thermistor strings T-3 and T-2 indicates that for this particular set of thermo-hydraulic soil properties in Figure 1, the zone of influence of degree of saturation changes is relatively limited in the conglomerate material. The effect of the changes in degree of saturation with heating can be further investigated using the numerical simulation results through the radial distributions in degree of saturation, thermal conductivity, and volumetric heat capacity at the end of the heat injection period shown in

Figures 18(a), 18(b), and 18(c), respectively. Decreases in all three variables are noticed at the end of heating, with greater decreases at the locations of the borehole heat exchangers. The radial distributions for degree of saturation differ from those for the temperature observed in Figure 15, which reflect a clear overlapping effect between the borehole heat exchangers. Zones of influence of changes in degree of saturation of approximately 0.3 m is observed around borehole heat exchanger A and of approximately 0.25 m is observed around borehole heat exchanger B, which was not sufficient to cause a significant overlapping effect between the two boreholes. Although not investigated, repeated cycles of heat injection and heat removal may leader to greater zones of influence. Similar to the observations of Baser et al. (2018), greater decreases in degree of saturation are observed for the locations with initially greater degree of saturation and for greater changes in temperature, due to the effects of enhanced vapor diffusion and phase change. Another interesting observation is that the percent decrease in the thermal conductivity in Figure 18(b) is greater than the percent decrease in the volumetric heat capacity in Figure 18(c). This has positive implications on the performance of the heat storage systems as the lower thermal conductivity is expected to lead to decrease in the heat loss from the system while the volumetric heat capacity reflects the total heat that can be stored in the soil for a given increase in ground temperature.

Another comparison that can be made is the difference in the simulations expected for the subsurface having thermo-hydraulic properties representative of unsaturated and saturated conditions. When the subsurface is saturated, the governing equations in Table 1 are significantly simplified. Heat transfer will occur primarily due to conduction, but natural convection of the pore water will occur due to decreases in the density of water with temperature. A comparison of the simulations for saturated and unsaturated conditions along with the measured ground temperatures are shown in Figure 19 for a depth near the upper-middle of the array at the location of borehole T-2. The temperature for saturated conditions are generally lower, although they tend to rise sharply near the end of the heat injection period, possibly due to upward water flow due to natural convection. Further comparisons of the model for saturated and unsaturated conditions are shown in Baser et al. (2018) for the case of a single geothermal heat exchanger.

6. CONCLUSIONS

This study focused on the simulation of transient heat transfer and water flow in a field-scale SBTES system installed in the vadose zone. A non-isothermal, coupled heat transfer and water flow model considering enhanced vapor diffusion and nonequilibrium phase change calibrated in the laboratory using reconstituted specimens collected from the field was validated by comparing simulated ground temperatures with those from field-scale SBTES system during both heat injection and ambient cooling. In general, a good match was obtained between the simulated and measured temperature data, reflecting the importance of considering coupled heat transfer and water flow when simulating SBTES systems installed in the vadose zone. During heat injection, ground temperatures were generally greater near the surface in the borehole array, likely due to heat transfer due to buoyancy-driven vapor flow. At the end of 5 months of ambient cooling, some heat was still retained within the array, indicating that further heat injection and cooling cycles would lead to a positive effect on the performance of this heat storage approach.

Differences between the simulation and measured data were likely due to differences in how the heat injection boundary conditions were applied, the assumption of a homogenous subsurface, the calibration of the model parameters using reconstituted specimens, and the assumption regarding the depth of the water table (which may vary with time). Heat transfer led to a clear overlapping effect between the closely-spaced geothermal borehole heat exchangers in the SBTES system. However, the simulation results indicate that a significant overlapping effect was not observed in terms of the changes in degree of saturation between the geothermal borehole heat exchangers. Permanent decreases in degree of saturation were observed at the locations of the geothermal heat exchangers, corresponding to a decrease in thermal conductivity, but similar decreases in these variables were not observed in the bulk of the subsurface between the geothermal borehole heat exchangers for the particular conditions at the site. Further study on the effects of heating and cooling cycles of SBTES systems in the vadose zone may better clarify the roles of thermo-hydraulic interaction between closely spaced geothermal borehole heat exchangers for different subsurface materials.

ACKNOWLEDGEMENTS

Funding provided by National Science Foundation grant 1230237 is much appreciated. The opinions presented here belong to authors alone.

REFERENCES

Akrouch, G.A., Sánchez, M., and Briaud, J.L. (2016). “An experimental, analytical and numerical study on the thermal efficiency of energy piles in unsaturated soils.” Computers and Geotechnics. 71, 207-220.

Baser, T. and McCartney, J.S. (2015a). "Development of a full-scale soil-borehole thermal energy storage system." Proc. Int. Foundation Conference and Equipment Exposition (IFCEE 2015). ASCE, Reston, VA. pp. 1608-1617.

Başer, T. and McCartney, J.S. (2015b). "Thermal energy storage in borehole arrays." Symposium on Energy Geotechnics. Barcelona. Jun. 2-4. pp. 1-2.

Baser, T., Lu, N., and McCartney, J.S. (2016a). "Operational response of a soil-borehole thermal energy storage system." ASCE Journal of Geotechnical and Geoenvironmental Engineering. 04015097-1-12. 10.1061/(ASCE)GT.1943-5606.0001432.

Baser, T., McCartney, J.S., Moradi, A., Smits, K., and Lu, N. (2016b). "Effect of a thermo-hydraulic insulating layer on the long-term response of soil-borehole thermal energy storage systems". GeoChicago 2016: Sustainability, Energy and the Geoenvironment. Chicago. Aug. 14-18. ASCE, Reston, VA. pp. 125-134.

Baser, T., Dong, Y., and McCartney, J.S. (2016c). "Heat content in soil-borehole thermal energy systems in the vadose zone." ICEGT 2016: 1st International Conference on Energy Geotechnics. Kiel. CRC Press, Boca Raton. pp. 195-202.

Baser, T., Dong, Y., Lu, N., and McCartney, J.S. (2016d). "Role of considering non-constant soil thermal parameters in the simulation of geothermal heat storage systems in the vadose zone". Proceedings. 8th Asian Young Geotechnical Engineers Conference 2016 (AYGEC 2016). Kazakh Geotechnical Society. Astana. pp. 1-6.

Başer, T., Dong, Y., Moradi, A.M., Lu, N., Smits, K., Ge, S., Tartakovsky, D., and McCartney, J.S. (2018). "Role of water vapor diffusion and nonequilibrium phase change in geothermal energy storage systems in the vadose zone." Journal of Geotechnical and Geoenvironmental Engineering. 10.1061/(ASCE)GT.1943-5606.0001910.

Baser, T., Hanna, C., and McCartney, J.S. (2019). "Performance of a field-scale shallow horizontal thermal energy storage system." Geo-Congress 2019: The 8th International Conference on Case Histories in Geotechnical Engineering. Philadelphia, PA. Mar. 24-27. 1-10. Accepted.

Bear, J. (1972). Dynamics of Fluids in Porous Media. Dover, Mineola, N.Y., 764.

Bjoern, H. (2013). "Borehole thermal energy storage in combination with district heating." EGC 2013. Pisa. June 3-7. 1-13.

Bixler, N.E. (1985). NORIA: "A Finite Element Computer Program for Analyzing Water, Vapor, Air and Energy Transport in Porous Media." SAND84-2057, Sandia National Laboratories, Albuquerque, NM.

Campbell, G.S. (1985). Soil Physics with BASIC: Transport Models for Soil–Plant Systems. Elsevier, New York.

Campbell, G.S., Jungbauer, J.D., Bidlake, W.R., and Hungerford, R.D. (1994). "Predicting the effect of temperature on soil thermal conductivity." Soil Science. 158, 307–313.

Cass, A., Campbell, G.S., and Jones. T.L. (1984.) "Enhancement of thermal water vapor diffusion in soil." Soil Science Society of America. 48(1), 25–32.

Catolico, N., Ge, S., and McCartney, J.S. (2016). "Numerical modeling of a soil-borehole thermal energy storage system." Vadose Zone Hydrology. 1-17.doi:10.2136/vzj2015.05.0078.

Choi, J.S., Lee, S.R., and Lee, D.S. (2011). “Numerical simulation of vertical ground heat exchangers: Intermittent operation in unsaturated soil conditions.” Computers and Geotechnics. 38, 949-958.

Claesson, J. and Hellström G. (1981). “Model studies of duct storage systems.” New Energy Conservation Technologies and their Commercialization. J.P. Millhone and E.H. Willis, Eds. Springer-Verlag, Berlin. 762-778.

COMSOL Multiphysics® v. 5.2. (2015). COMSOL AB, Stockholm, Sweden.

Ewen, J. and Thomas, H.R. (1989). “Heating unsaturated medium sand.” Géotechnique. 39(3), 455-470.

Gens, A., Garcia Molina, A., Olivella, S., Alonso, E.E., and Huertas, F. (1998). “Analysis of a full scale in-situ test simulating repository conditions.” International Journal of Numerical and Analytical Methods in Geomechanics. 22(7), 515–48.

Gens, A, Sanchez, M., Guimaraes L., and Huertas, F. (2009). “A full-scale in situ heating test for high-level nuclear waste disposal: Observations, analysis and interpretation.” Géotechnique, 59(4), 377-399.

Grant, S.A. and Salehzadeh, A. (1996). Calculations of temperature effects on wetting coefficients of porous solids and their capillary pressure functions. Water Resources Res. 32(2), 261-279.

Hillel, D. (1980). Fundamental of Soil Physics. Academic, San Diego, CA.

Iezzoni, H. M. and McCartney, J.S. (2016). “Calibration of Capacitance Sensors for Compacted Silt in Non-Isothermal Applications.” Geotechnical Testing Journal, Vol. 39(2), 169-180.

Lide, D.R. (Ed.) (2001). Handbook of Chemistry and Physics, CRC Press, Boca Raton, FL.

Lu, N. and Dong, Y. (2015). “A closed form equation for thermal conductivity of unsaturated soils at room temperature.” Journal of Geotechnical and Geoenvironmental Engineering. 141(6), 04015016.

Marcotte, D. and Pasquier, P. (2014). “Unit-response function for ground heat exchanger with parallel, series or mixed borehole arrangement.” Renewable Energy. 68, 14–24.

McCartney, J.S., Ge, S., Reed, A., Lu, N., and Smits, K. (2013). “Soil-borehole thermal energy storage systems for district heating.” Proceedings of the European Geothermal Congress 2013. Pisa. Jun. 3-7. pp. 1-10.

Millington, R.J., and Quirk, J.M. (1961). “Permeability of porous solids.” Trans. Faraday Soc. 57, 1200–1207.

Moradi, A.M., Smits, K., Lu, N., and McCartney, J.S. (2016). “3-D experimental and numerical investigation of heat transfer in unsaturated soil with an application to soil borehole thermal energy storage (SBTES) systems.” Vadose Zone J. 15(10), 1-17.

Nguyen, A., Pasquier, P., and Marcotte, D. (2017). “Borehole thermal energy storage systems under the influence of groundwater flow and time-varying surface temperature.” Geothermics. 66, 110-118.

Nordell, B. and Hellström, G. (2000). “High temperature solar heated seasonal storage system for low temperature heating of buildings.” Applied Energy. 69(6), 511–523.

Nussbicker-Lux, J. (2012). “The BTES project in Crailsheim (Germany) – Monitoring results.” Proc. 12th Int. Conf. on Energy Storage – Innostock. IEA Press, Paris. 1-10.

Sibbitt, B., McClenahan, D., Djebbar, R., Thornton, J., Wong, B., Carriere, J., Kokko, J. (2012). “The performance of a high solar fraction seasonal storage district heating system - Five years of operation.” Energy Procedia. 30, 856-865.

Smits, K.M., Cihan, A., Sakaki, S., and Illangasekare, T.H. (2011). “Evaporation from soils under thermal boundary conditions: Experimental and modeling investigation to compare equilibrium- and nonequilibrium-based approaches.” Water Resources Research. 47, W05540, doi:10.1029/2010WR009533.

Thomas, H.R. and Sansom, M.R. (1995). “Fully coupled heat, moisture, and air transfer in an unsaturated soil.” J Eng Mech 1995;12(3):392–405.

Thomas, H.R. and Rees, S.W. (2009). “Measured and simulated heat transfer to foundation soils.” Géotechnique. 59(4), 365–375.

van Genuchten, M.T. (1980). “A closed-form equation for predicting the hydraulic conductivity of unsaturated soils.” Soil Sci. Soc. Am. J. 44(5), 892–898.

Wayllace, A. and Lu, N. (2012). “A transient water release and imbibitions method for rapidly measuring wetting and drying soil water retention and hydraulic conductivity functions.” Geotechnical Testing Journal. 35(1), 103-117.

Welsch, B., Rühaak, W., Schulte, D.O., Bär, K., Homuth, S., and Sass, I. (2015). “Comparative study of medium deep borehole thermal energy storage systems using numerical modelling.” Proc. World Geothermal Congress 2015. International Geothermal Association. Bochum. 1-6.

Whitaker, S. (1977). “Simultaneous heat, mass and momentum transfer in porous media: A theory of drying porous media.” Adv. Heat Transf. 13, 119–203.

TABLE 1. Equations used in the numerical analyses

Equation	Number	Reference
Nonisothermal liquid flow governing equation: $nS_{rw}\frac{\partial \rho_w}{\partial t}+n\rho_w\frac{dS_{rw}}{dP_c}\frac{\partial P_c}{\partial t}+\nabla\cdot\left[\rho_w\left(-\frac{k_{rw}\kappa}{\mu_w}\right)\nabla\left(P_w+\rho_w gz\right)\right]=-R_{gw}$ n=porosity (m^3/m^3), S_{rw}=degree of water saturation (m^3/m^3), ρ_w=temperature-dependent density of water (kg/m^3) (Hillel 1980), t=time(s), $P_c=P_w-P_g$=capillary pressure (Pa), P_w=pore water pressure (Pa), P_g=pore gas pressure (Pa), k_{rw}=relative permeability function for water (m/s); κ=intrinsic permeability (m^2); μ_w=temperature-dependent water dynamic viscosity (kg/(ms)) (Lide 2001), g=acceleration due to gravity (m/s^2) R_{gw}=Phase change rate (kg/m^3s)	(1)	(Bear 1972; Moradi et al. 2016)
Nonisothermal gas flow governing equation: $nS_{rg}\frac{\partial \rho_g}{\partial t}+n\rho_g\frac{dS_{rg}}{dP_c}\frac{\partial P_c}{\partial t}+\nabla\cdot\left[\rho_g\left(-\frac{k_{rg}\kappa}{\mu_g}\right)\nabla\left(P_g+\rho_g gz\right)\right]=R_{gw}$ S_{rg}=degree of gas saturation (m^3/m^3), ρ_g=temperature-dependent density of gas (kg/m^3) (Smits et al. 2011), k_{rg}=relative permeability function for gas (m/s); μ_g=temperature-dependent gas dynamic viscosity (kg/(ms))	(2)	(Bear 1972; Moradi et al. 2016)
Water vapor mass balance equation: $n\frac{\partial\left(\rho_g S_{rg} w_v\right)}{\partial t}+\nabla\cdot\left(\rho_g u_g w_v-D_e\rho_g\nabla w_v\right)=R_{gw}$ $D_e=D_v\tau$=effective diffusion coefficient (m^2/s), D_v=diffusion coefficient of water vapor in air (m^2/s) (Campbell 1985), w_v=mass fraction of water vapor in the gas phase (kg/kg), $\tau=n^{1/3}S_{rg}^{7/3}\eta$=tortuosity (Millington and Quirk 1961)	(3)	(Smits et al. 2011)
Enhancement factor for vapor diffusion, η: $\eta=a+3S_{rw}-(a-1)\exp\left\{-\left[\left(1+\frac{2.6}{\sqrt{f_c}}\right)S_{rw}\right]^3\right\}$ a=empirical fitting parameter representing the soil-specific enhancement in vapor diffusion, f_c= clay content	(4)	(Cass et al. 1984)
Nonequilibrium phase change rate, R_{gw}: $R_{gw}=\left(\frac{bS_{rw}RT}{M_w}\right)\left(\rho_{veq}-\rho_v\right)$ b=empirical fitting parameter representing the soil-specific nonequlibrium phase change rate (s/m^2), R=universal gas constant (J/molK), ρ_{veq}=equilibrium vapor density (kg/m^3) (Campbell 1985), T=Temperature (K), ρ_v=vapor density (kg/m^3), M_w=molecular weight of water (kg/mol)	(5)	(Bixler 1985; Moradi et al. 2016)
Heat transfer energy balance: $\left(\rho C_p\right)\frac{\partial T}{\partial t}+\nabla.\left(\left(\rho_w C_{pw}\right)u_w T+\left(\rho_g C_{pg}\right)u_g T-\left(\lambda\nabla T\right)\right)=-LR_{gw}+Q$ ρ=total density of soil (kg/m^3), C_p=specific heat of soil (J/kgK), C_{pw}=specific heat capacity of water (J/kgK), C_{pg}=specific heat capacity of gas (J/kgK), λ=thermal conductivity (W/mK), L=latent heat due to phase change (J/kg), u_w=water velocity (m/s), u_g=gas velocity (m/s), Q=heat source (W/m^3)	(6)	(Whitaker 1977; Moradi et al. 2016)

TABLE 2. Constitutive models used in the numerical analyses

Equation	**Number**	**Reference**
Soil Water Retention Curve (SWRC): $$S_{rw} = S_{rw,res} + \left(1 - S_{rw,res}\right)\left[\frac{1}{1+\left(\alpha_{vG} P_c(T)\right)^{N_{vG}}}\right]^{1-1/N_{vG}}$$ where $S_{rw,res}$ is the residual degree of saturation to water, α_{vG} and NvG are parameters representing the air entry pressure and the pore size distribution, respectively, and Pc(T) is the temperature-corrected capillary pressure according to the model of Grant and Salehzadeh (1996)	(7)	(van Genuchten 1980)
Hydraulic Conductivity Function (HCF): $$k_{rw} = \sqrt{\left(\frac{S_{rw} - S_{rw,res}}{1 - S_{rw,res}}\right)}\left[1 - \left(1 - \left(\frac{S_{rw} - S_{rw,res}}{1 - S_{rw,res}}\right)^{1/(1-1/N_{vG})}\right)^{1-1/N_{vG}}\right]^2$$ where α_{vG} and NvG are the same parameters as in Equation (7)	(8)	(van Genuchten 1980; Mualem 1970)
Thermal Conductivity Function (TCF): $$\frac{\lambda - \lambda_{\text{dry}}}{\lambda_{\text{sat}} - \lambda_{\text{dry}}} = 1 - \left[1 + \left(\frac{S_e}{S_{\text{f}}}\right)^m\right]^{1/m-1}$$ where λ_{dry} and λ_{sat} are the thermal conductivities of dry and saturated soil specimens, respectively, S_e is the effective saturation, S_f is the effective saturation at which the funicular regime is onset, and m is defined as the pore fluid network connectivity parameter for thermal conductivity	(9)	(Lu and Dong 2015)
Volumetric Heat Capacity Function (VHCF): $$\frac{C_v - C_{v\text{dry}}}{C_{v\text{sat}} - C_{v\text{dry}}} = 1 - \left[1 + \left(\frac{S_e}{S_{\text{f}}}\right)^m\right]^{1/m-1}$$ where C_{vdry} and C_{vsat} are the volumetric heat capacities of dry and saturated soil, respectively, and are similarly treated as fitting parameters, and S_f and *m* are the same parameters as in Equation (9)	(10)	(Baser et al. 2016b)

LIST OF FIGURE CAPTIONS

FIG. 1. Coupled thermo-hydraulic constitutive relationships for the UCSD conglomerate: (a) SWRC and HCF; (b) TCF and VHCF

FIG. 2. Schematic of the compaction mold used for calibration of water vapor diffusion and phase change parameters along with the location of the embedded sensor and its zone of influence

FIG. 3. Calibration of the numerical model parameters using the heating test on compacted soil (soil values at the depth of the dielectric sensor in Fig. 2): (a) Temperature; (b) Degree of saturation

FIG. 4. Experimental setup for the SBTES system: (a) Plan view; (b) Elevation view

FIG. 5. Photos of the SBTES system: (a) Excavation with borehole connections; (b) Hydraulic barrier; (c) Insulation layer

FIG. 6. Plan view of the BTES and the simulated model domain (temperature sensors in boreholes 1, 2, 3, and 4, heat exchangers in boreholes A through M)

FIG. 7. Initial and boundary conditions on the quarter domain model for a field-scale geothermal heat exchanger (JC is mass flux, distances in meters): (a) Thermal; (b) Hydraulic

FIG. 8. Thermal input boundary conditions to the SBTES system: (a) Ambient air temperature; (b) Solar thermal heat transfer rates; (c) Close-up of daily solar thermal heat transfer rates; (d) Energy balance

FIG. 9. Picture of borehole heat exchanger configuration highlighting heat injection sequence into Loops 1, 2, and 3 (Note: picture taken before inlet/outlet connections to manifold installed);

FIG. 10. Vertical SBTES loop heat transfer rates used in the calculations of the individual borehole boundary conditions: (a) Loop 1; (b) Loop 2; (c) Loop 3

FIG. 11. Predicted and measured temperature time series from thermistor string T-1 for different depths (z): (a) 16.00m; (b) 14.78m; (c) 12.95m; (d) 9.29m; (e) 6.85m; (f) 1.82m

FIG. 12. Predicted and measured temperature time series from thermistor string T-2 for different depths (z): (a) 16.00m; (b) 14.78m; (c) 12.95m; (d) 9.29m; (e) 6.85m; (f) 1.82m

FIG. 13. Predicted and measured temperature time series from thermistor string T-3 for different depths (z): (a) 16.00 m; (b) 14.78 m; (c) 12.95 m; (d) 9.29 m; (e) 6.85 m; (f) 1.82 m

FIG. 14. Predicted and measured temperature time series from thermistor string T-4 for different depths (z): (a) 16.00 m; (b) 14.78 m; (c) 12.95 m; (d) 9.29 m; (e) 6.85 m; (f) 1.82 m

FIG. 15. Radial temperature profiles at different depths (z): (a) At the end of heating; (b) After 5 months of ambient cooling

FIG. 16. Temperature profiles along the borehole length: (a) Borehole 2; (b) Borehole 4

FIG. 17. Time series of predicted degrees of saturation at the radial locations of: (a) Borehole 3; (b) Borehole 2

FIG. 18. Radial profiles of predicted values at the end of heating: (a) Degree of saturation; (b) Thermal conductivity; (c) Volumetric heat capacity

FIG. 19. Comparison of the transient temperature response of the subsurface having thermo-hydraulic properties representative of saturated and unsaturated conditions

Figure 1

Click here to download high resolution image

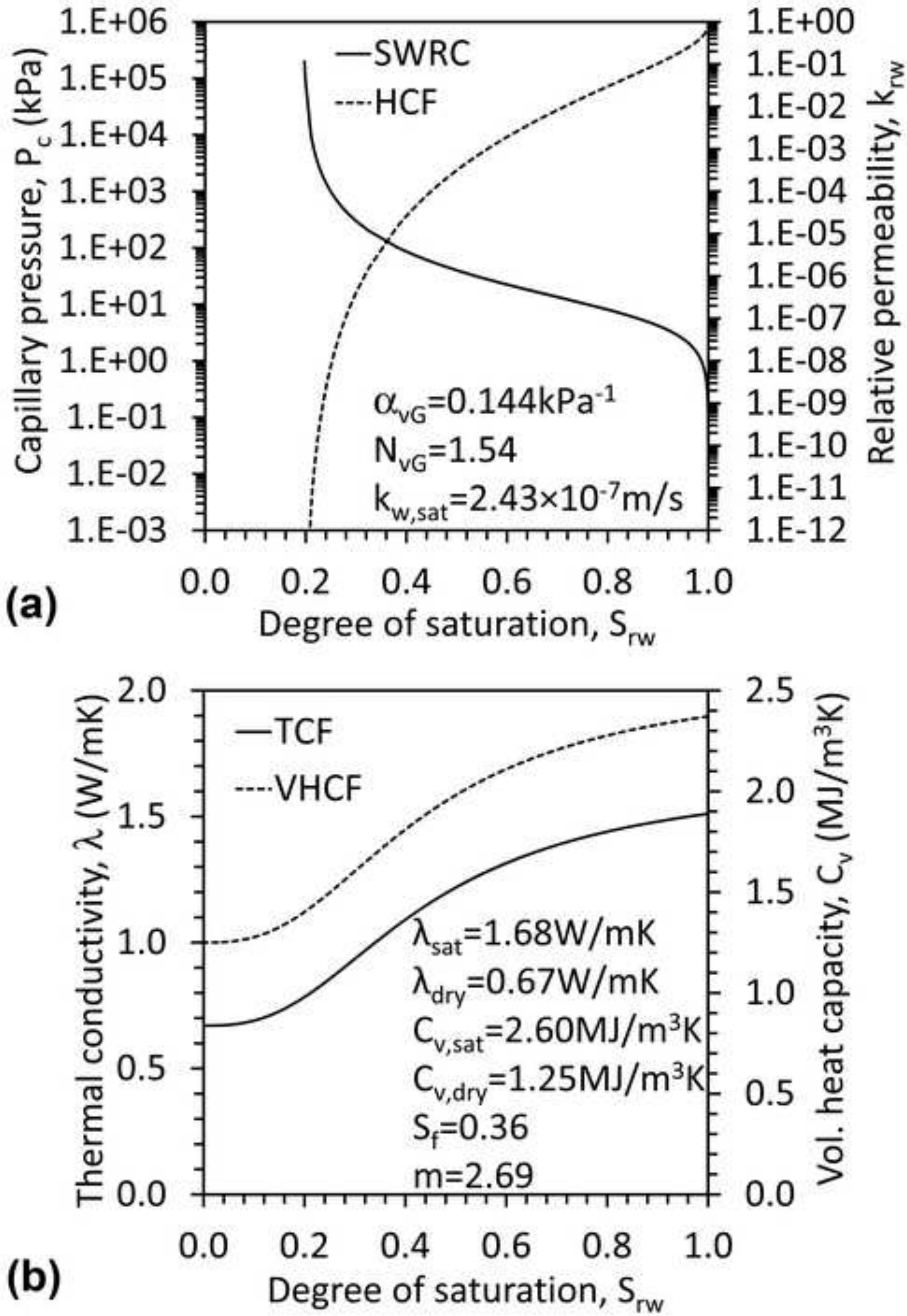

Figure 2

Click here to download high resolution image

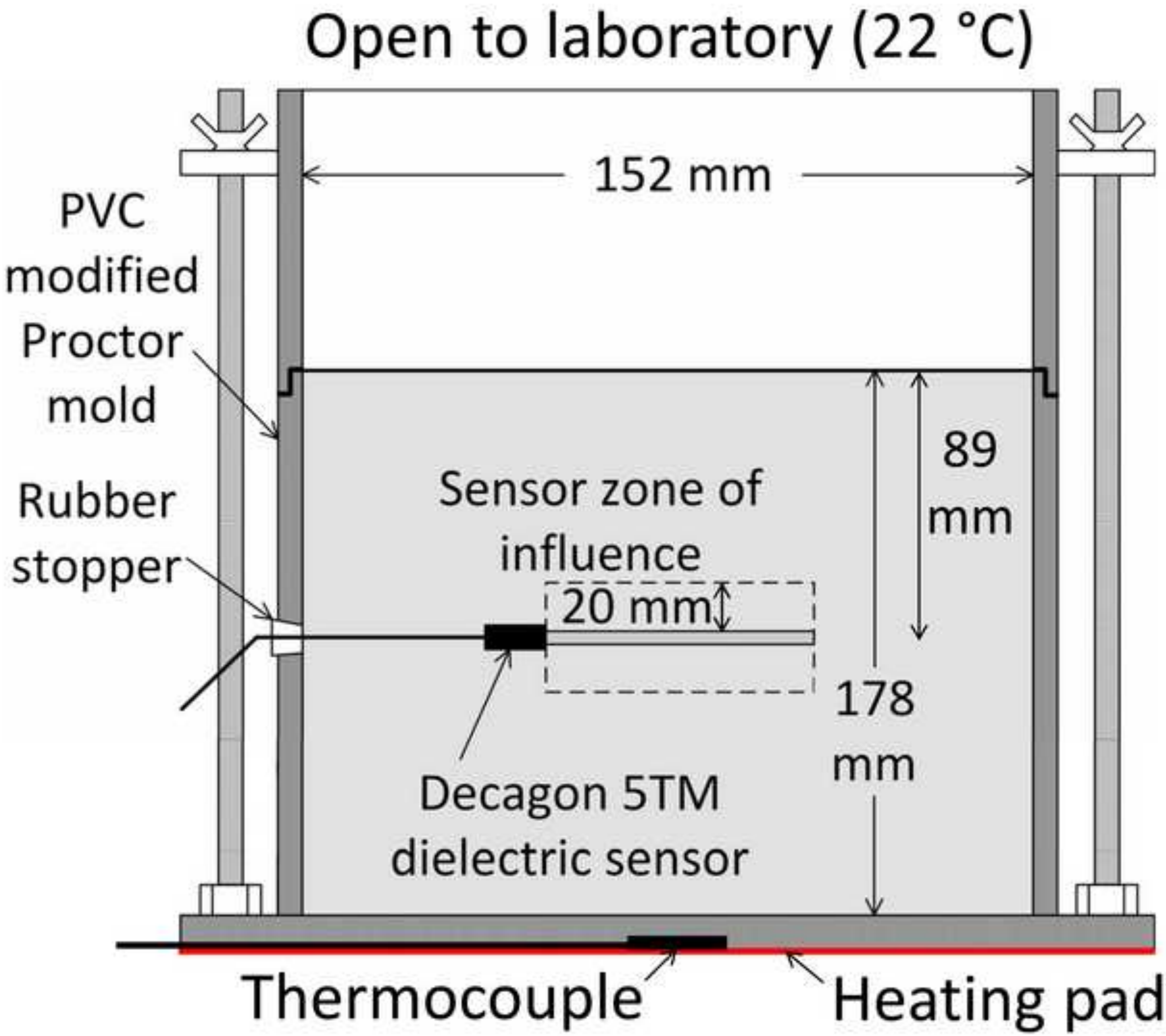

Figure 3
Click here to download high resolution image

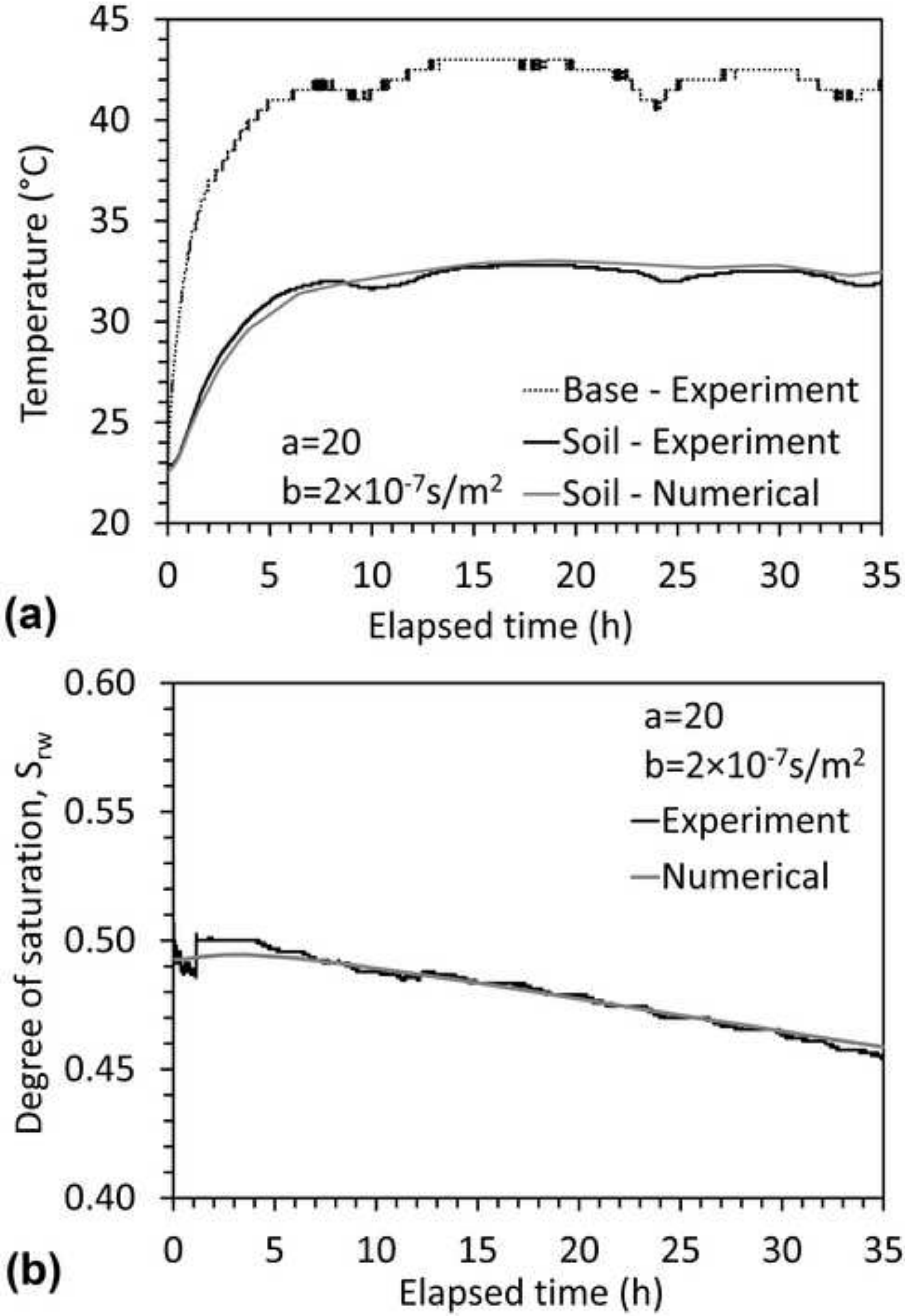

Figure 4
Click here to download high resolution image

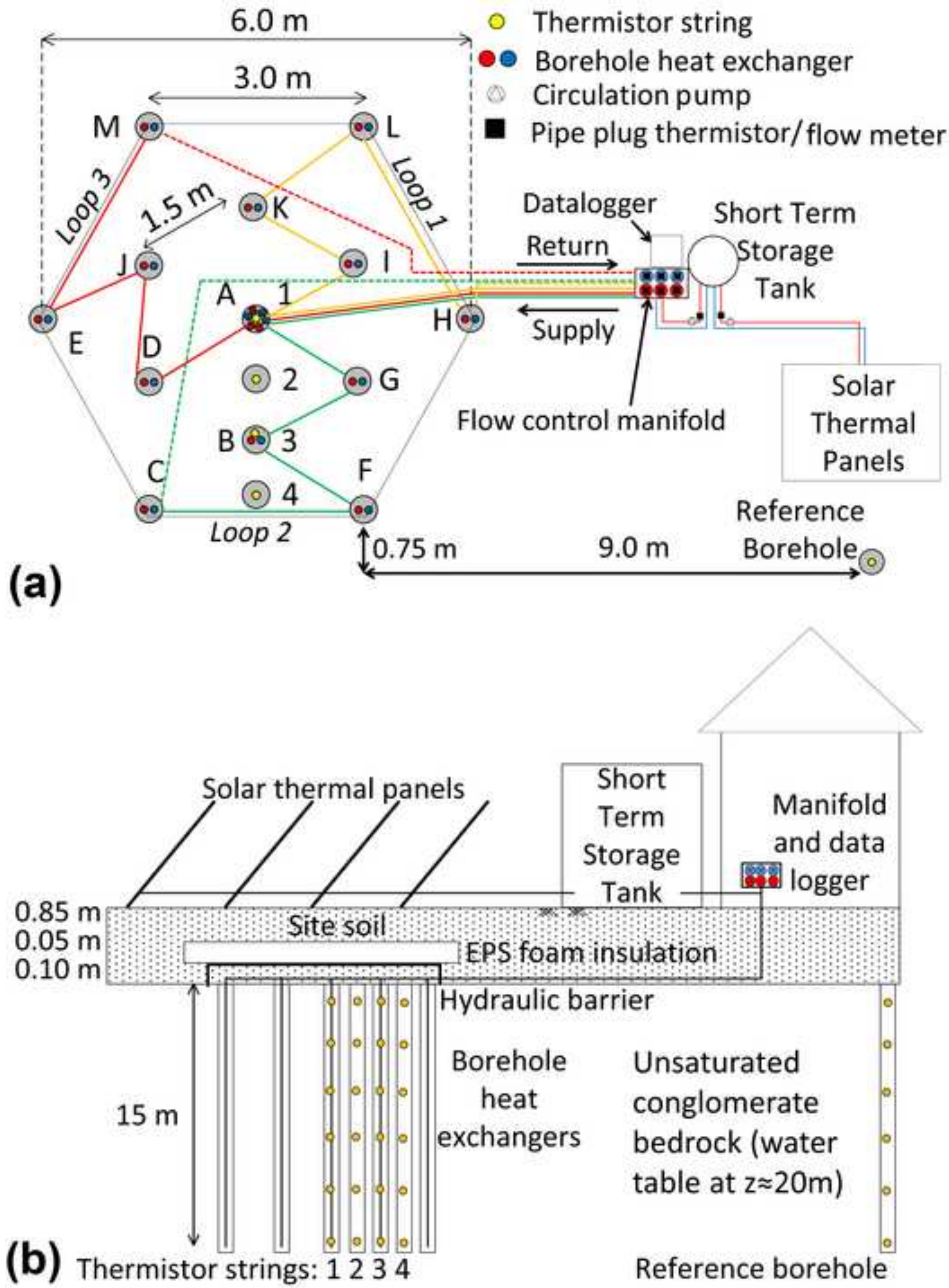

Figure 5

Click here to download high resolution image

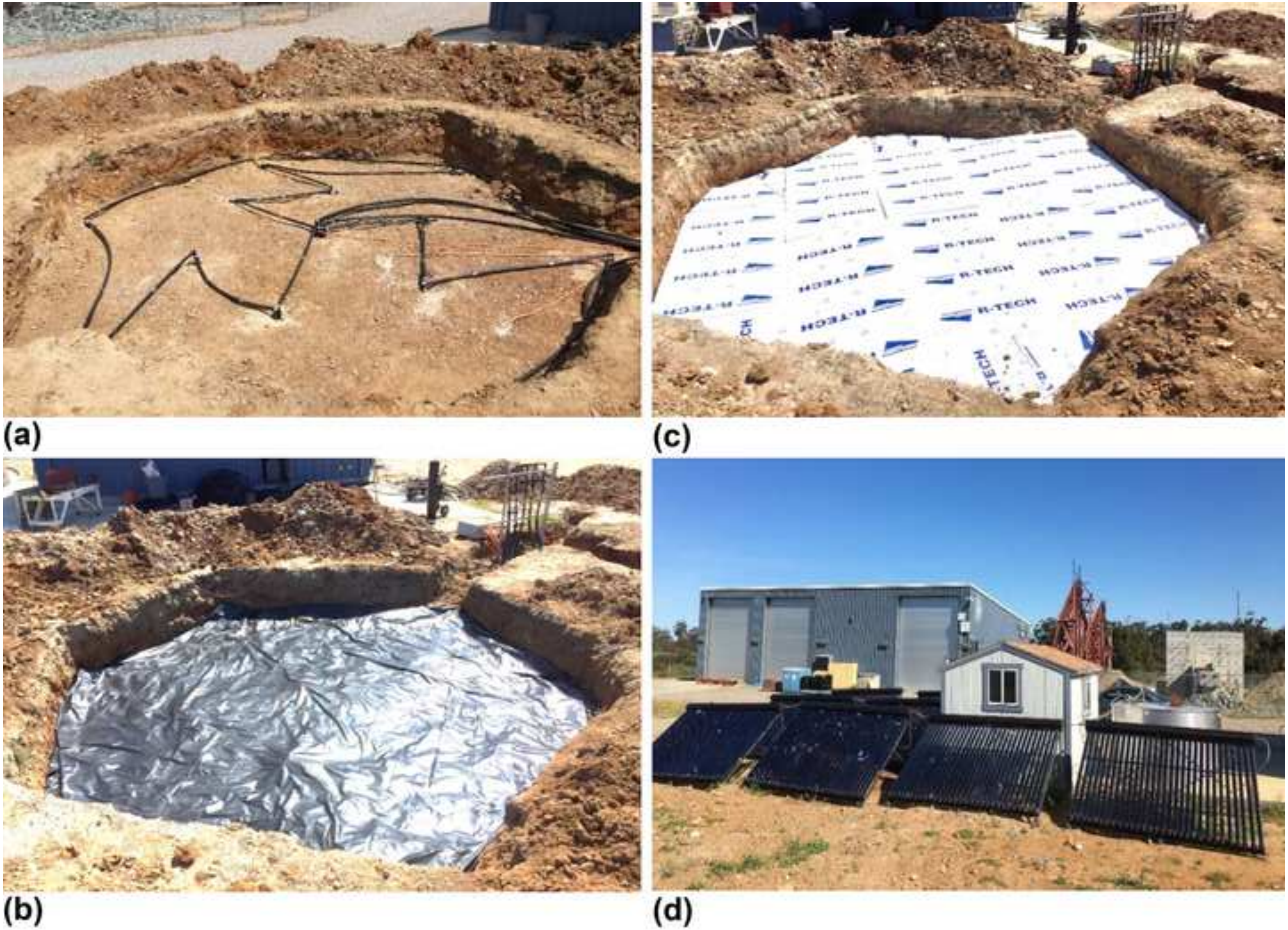

Figure 6

Click here to download high resolution image

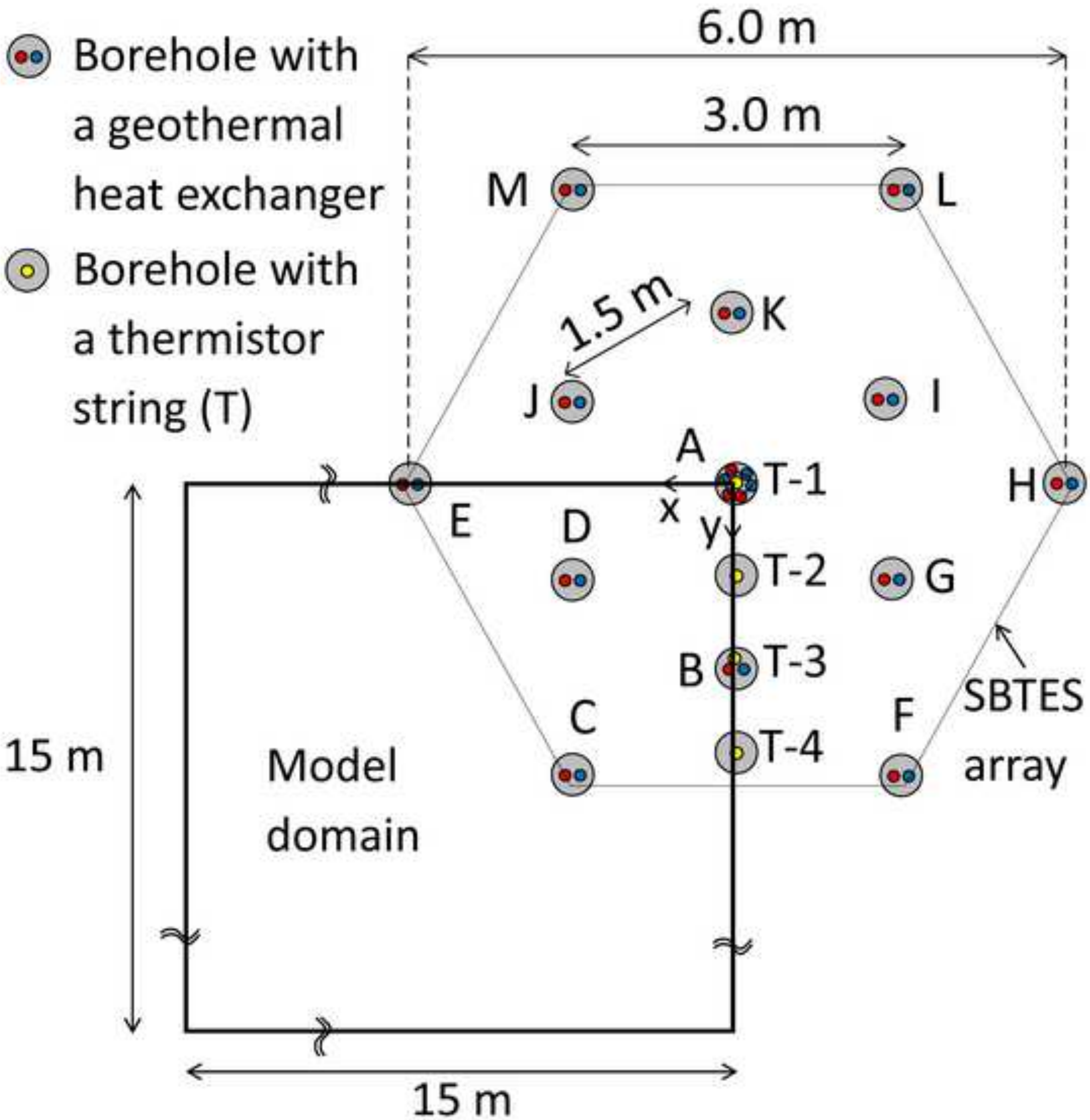

Figure 7

Click here to download high resolution image

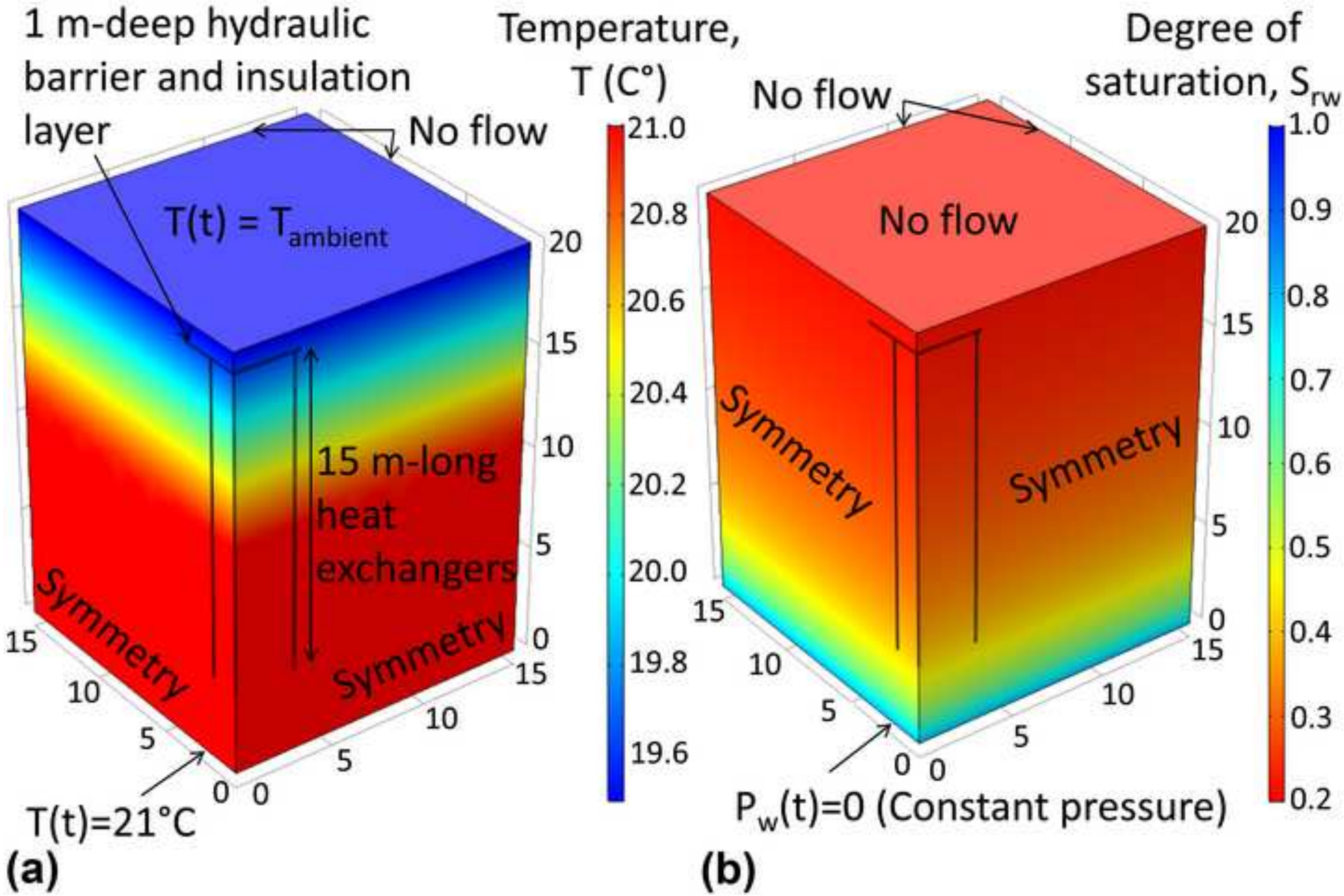

Figure 8

Click here to download high resolution image

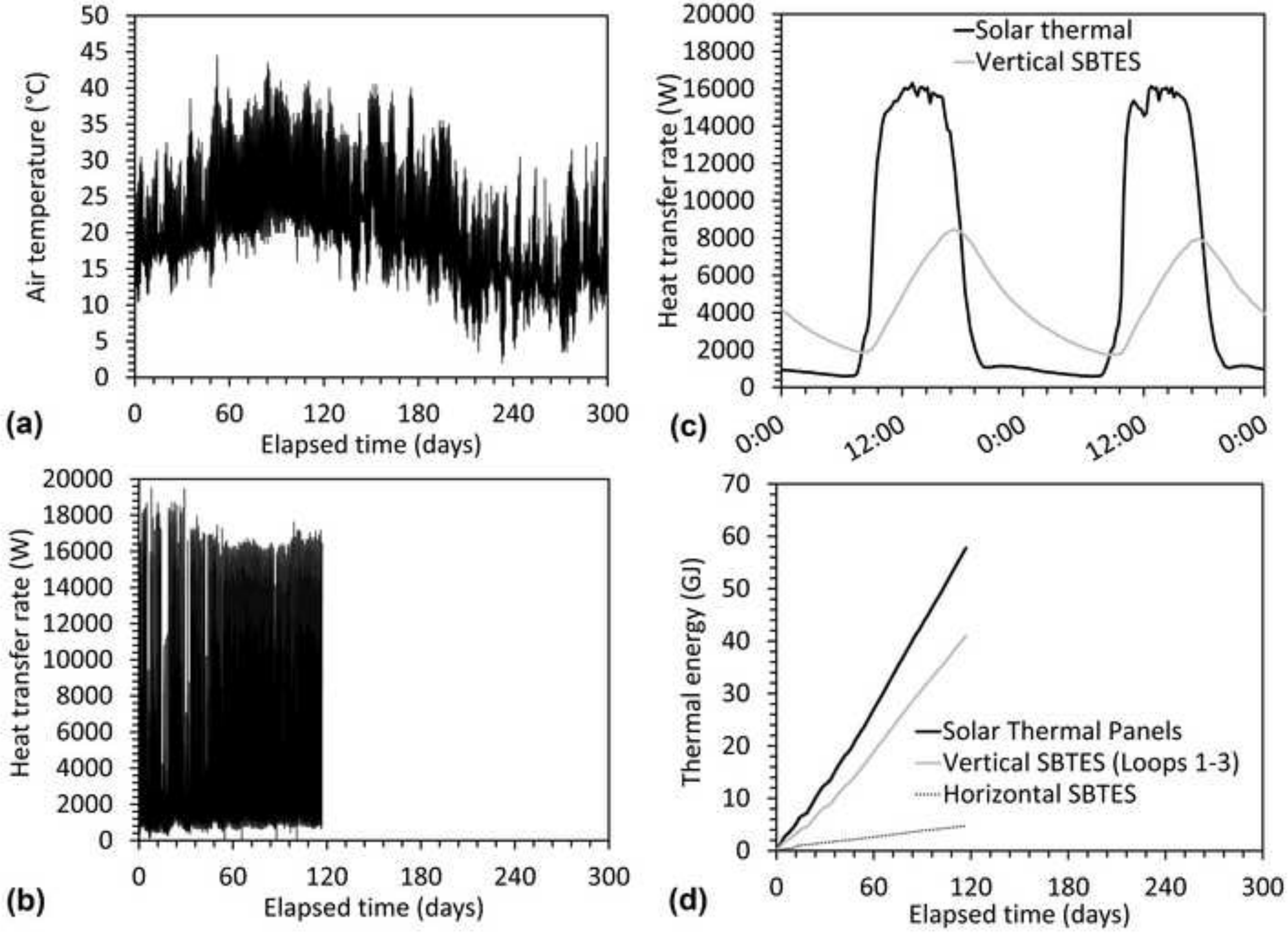

Figure 9
Click here to download high resolution image

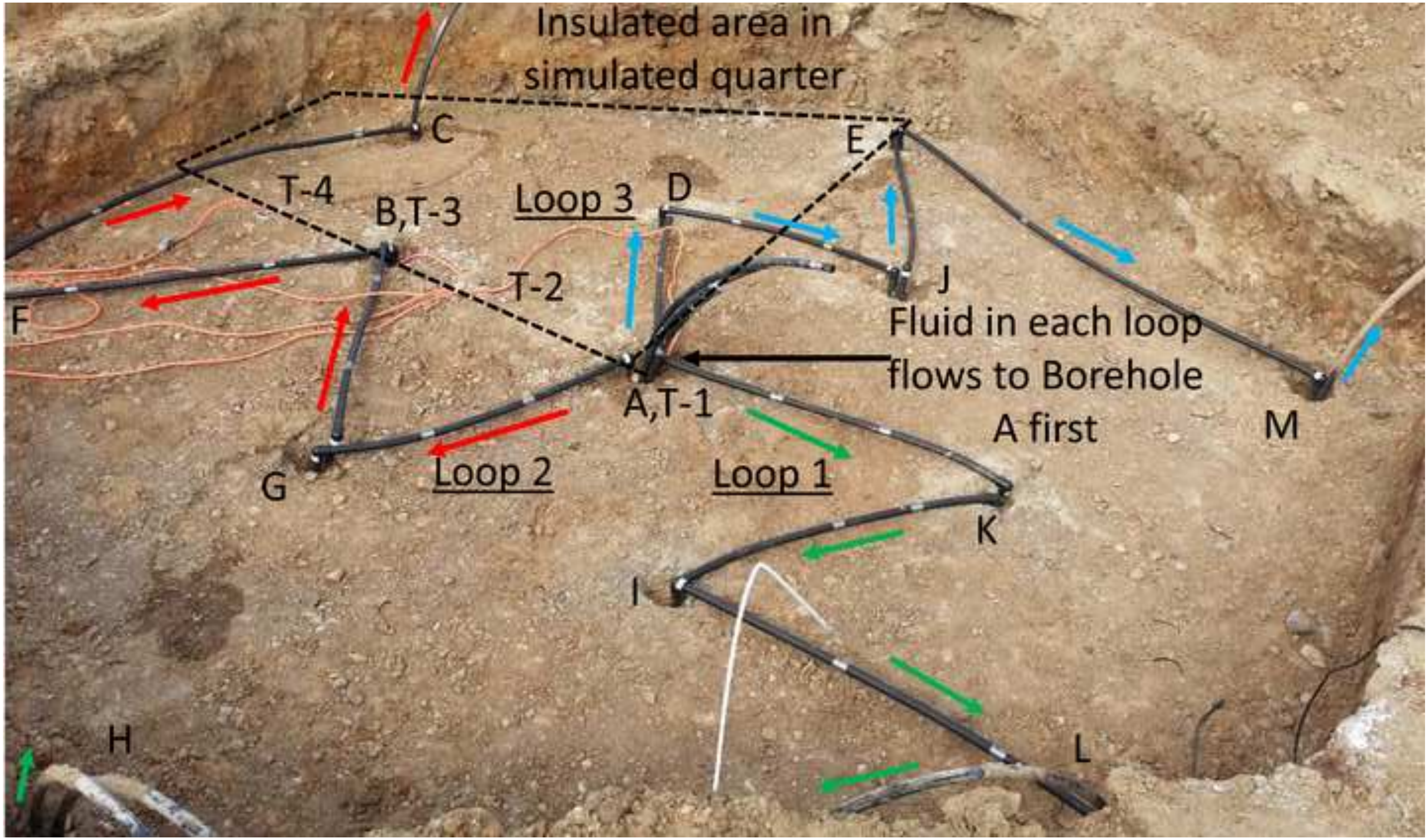

Figure 10
Click here to download high resolution image

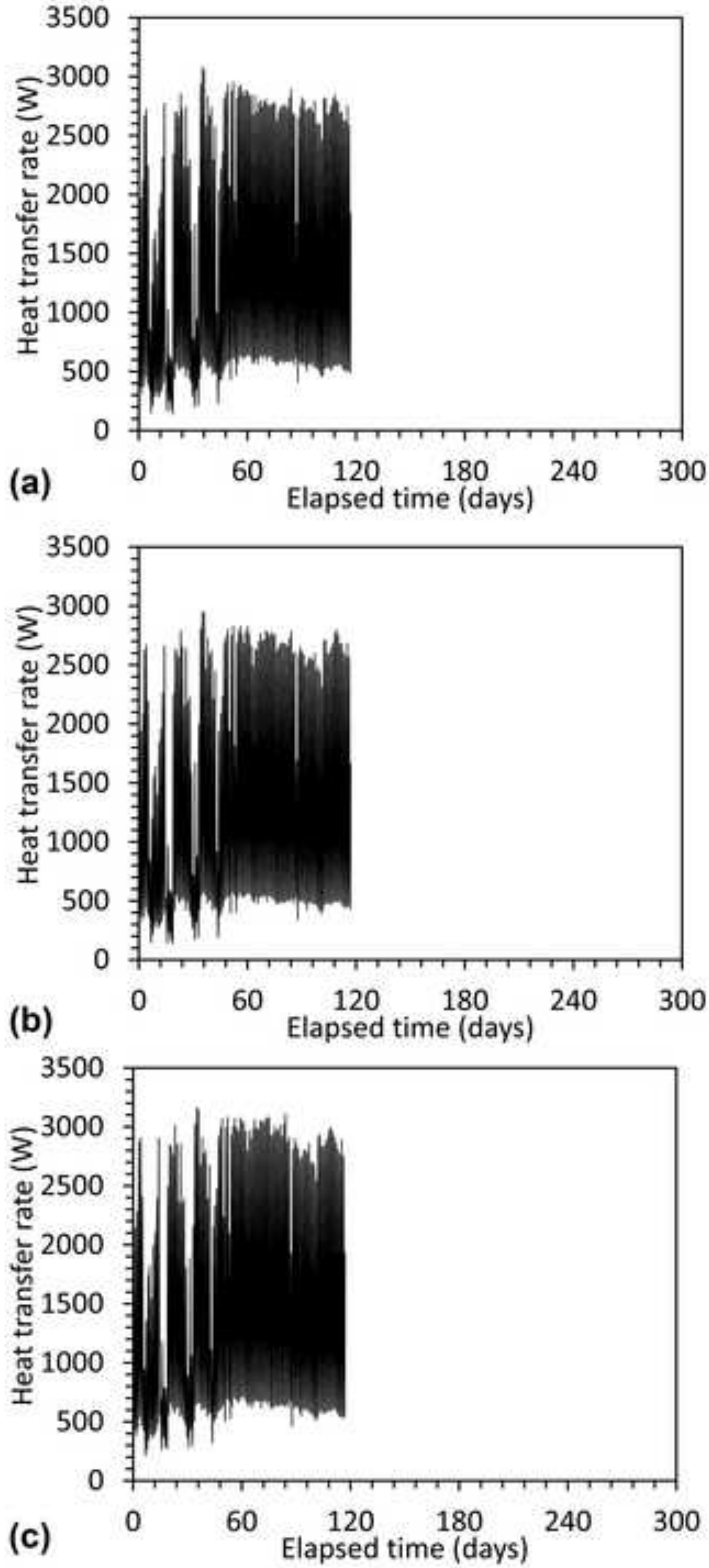

Figure 11
Click here to download high resolution image

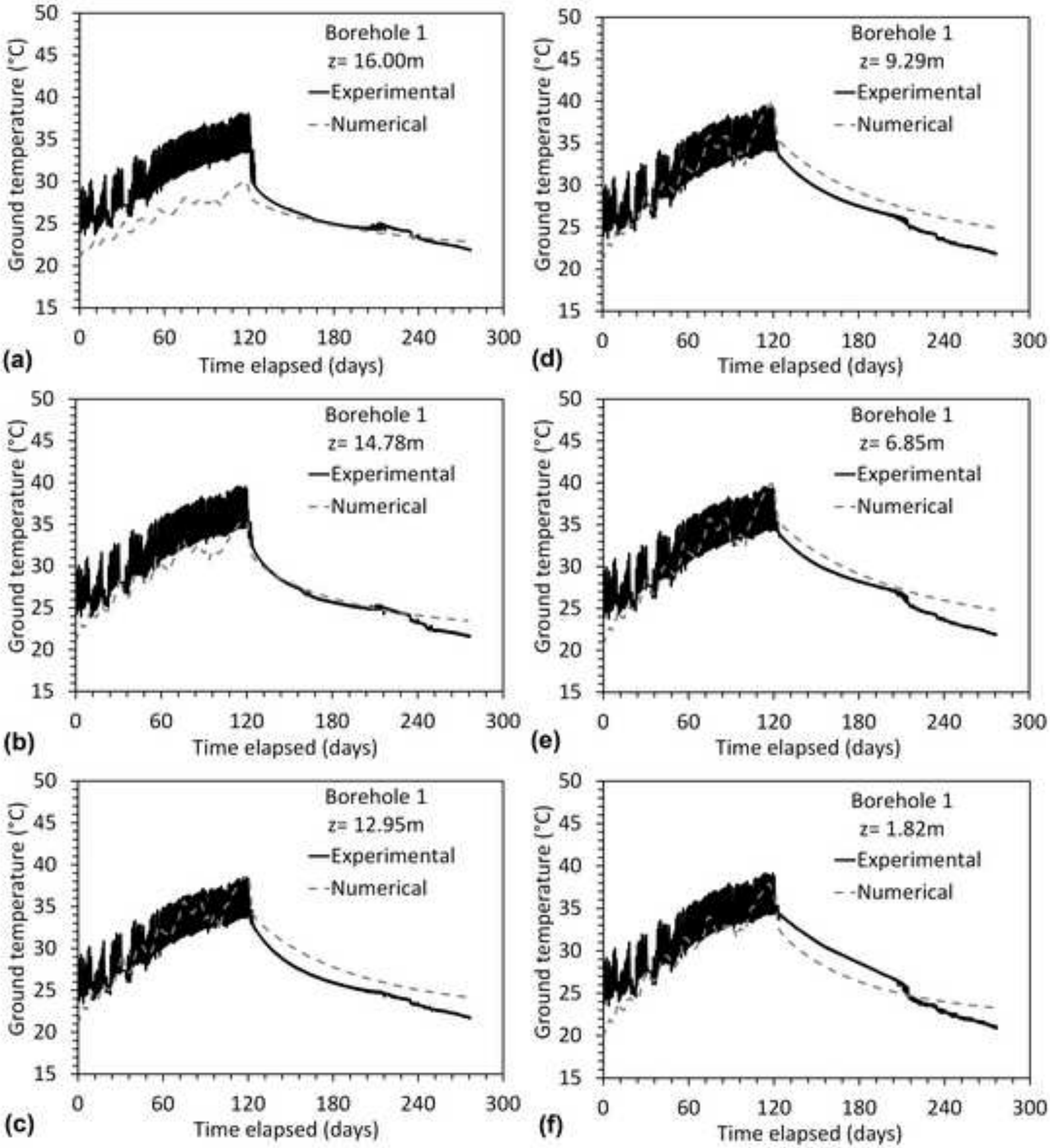

Figure 12
Click here to download high resolution image

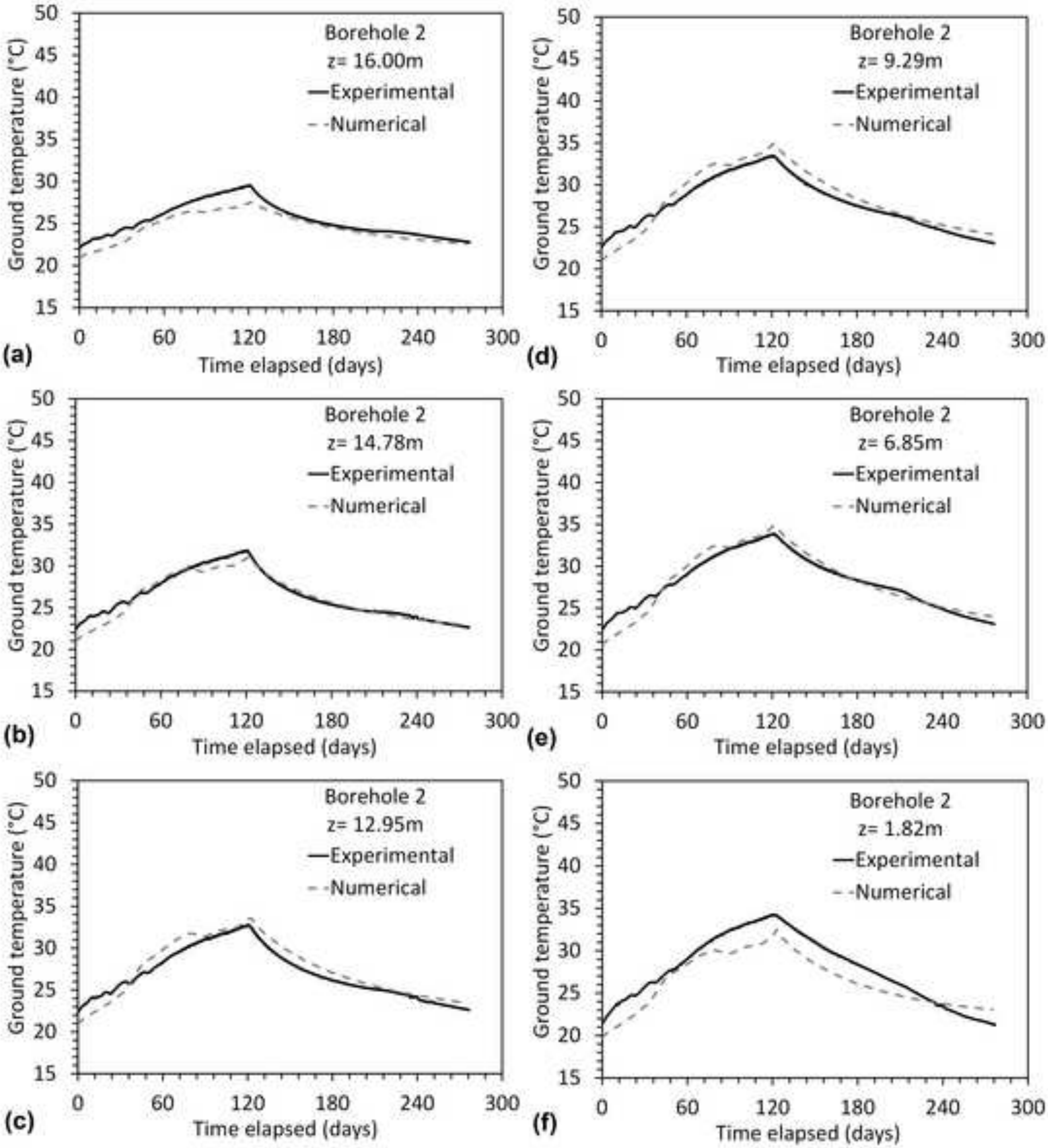

Figure 13
Click here to download high resolution image

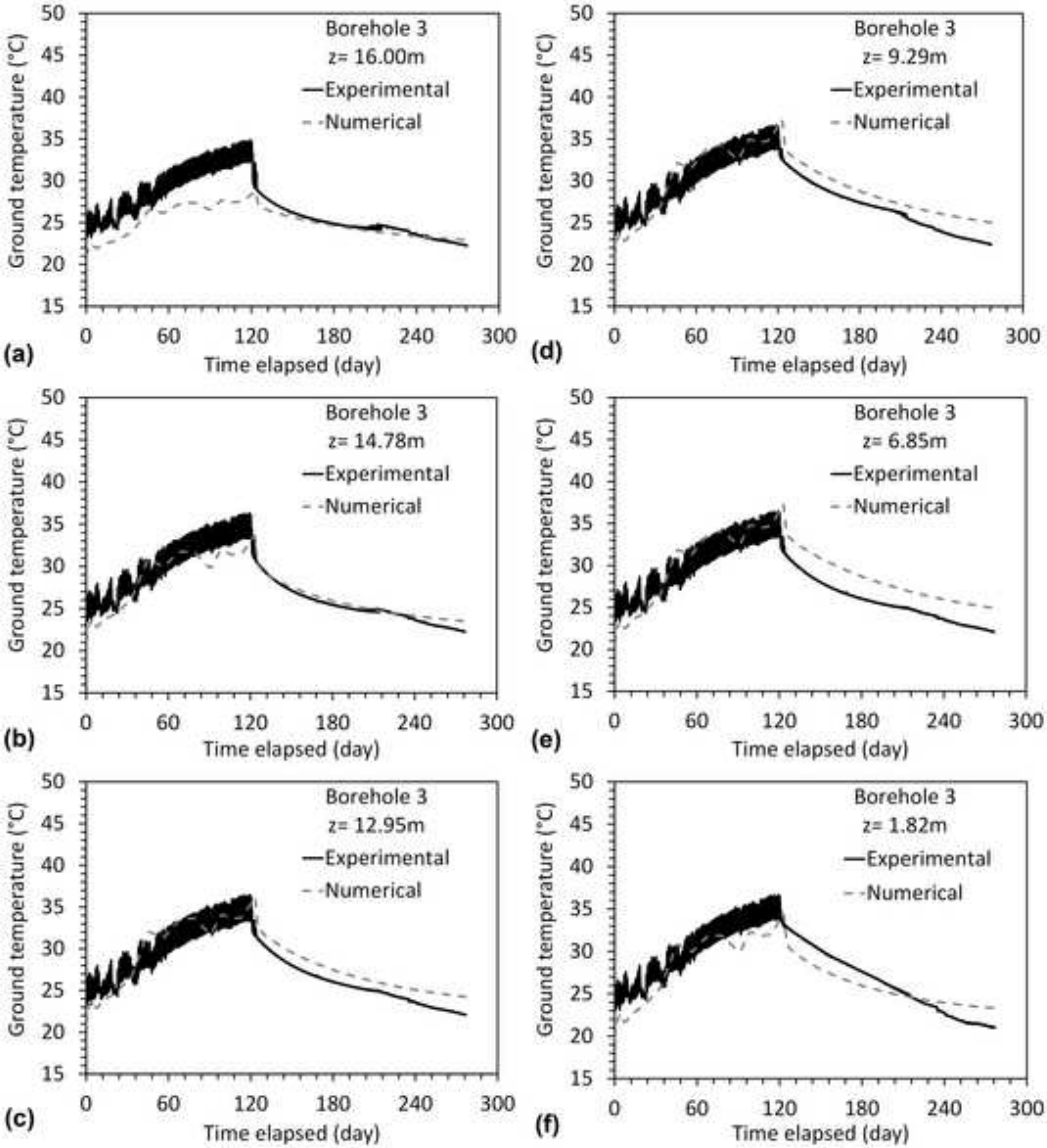

Figure 14
Click here to download high resolution image

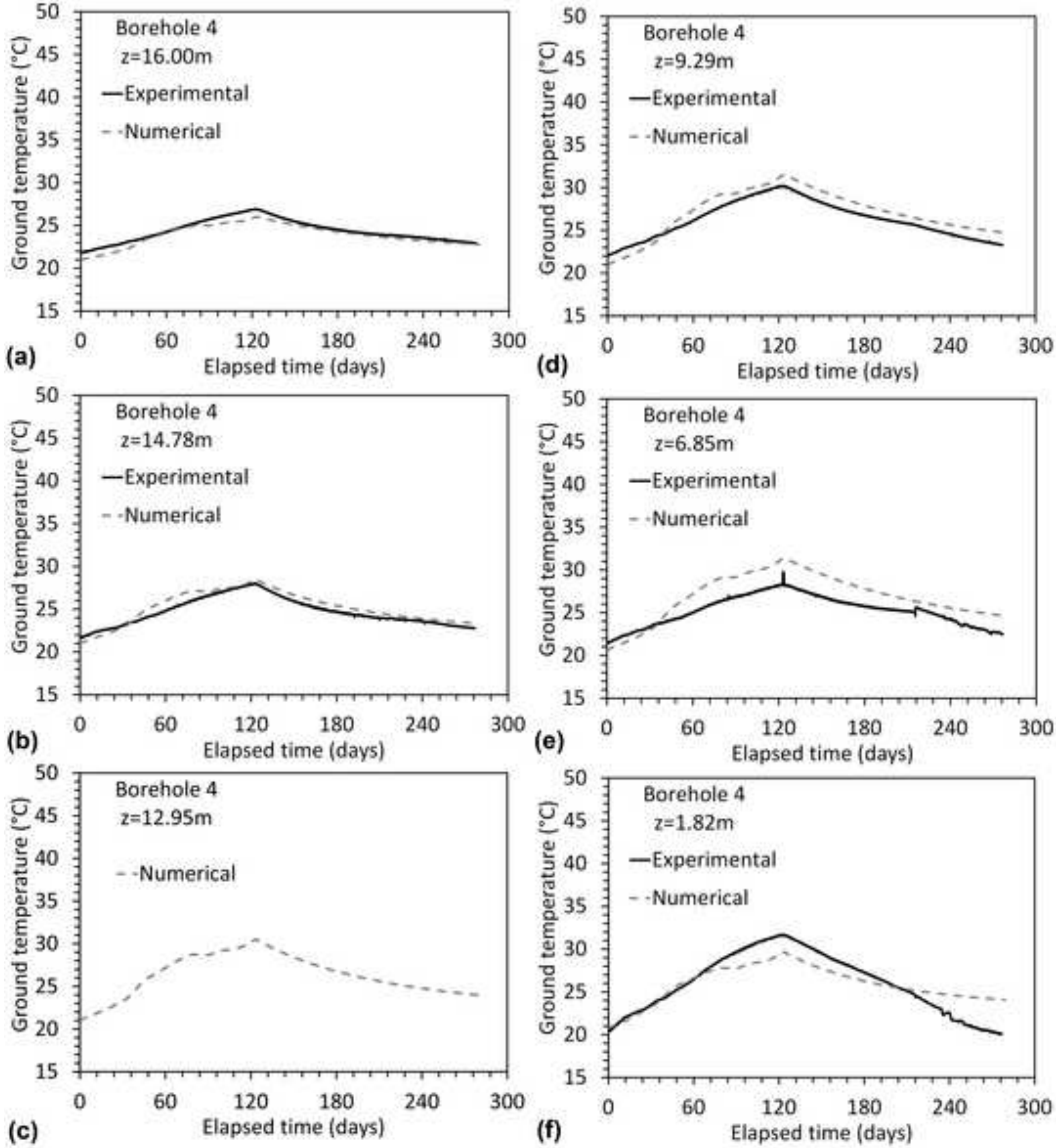

Figure 15
Click here to download high resolution image

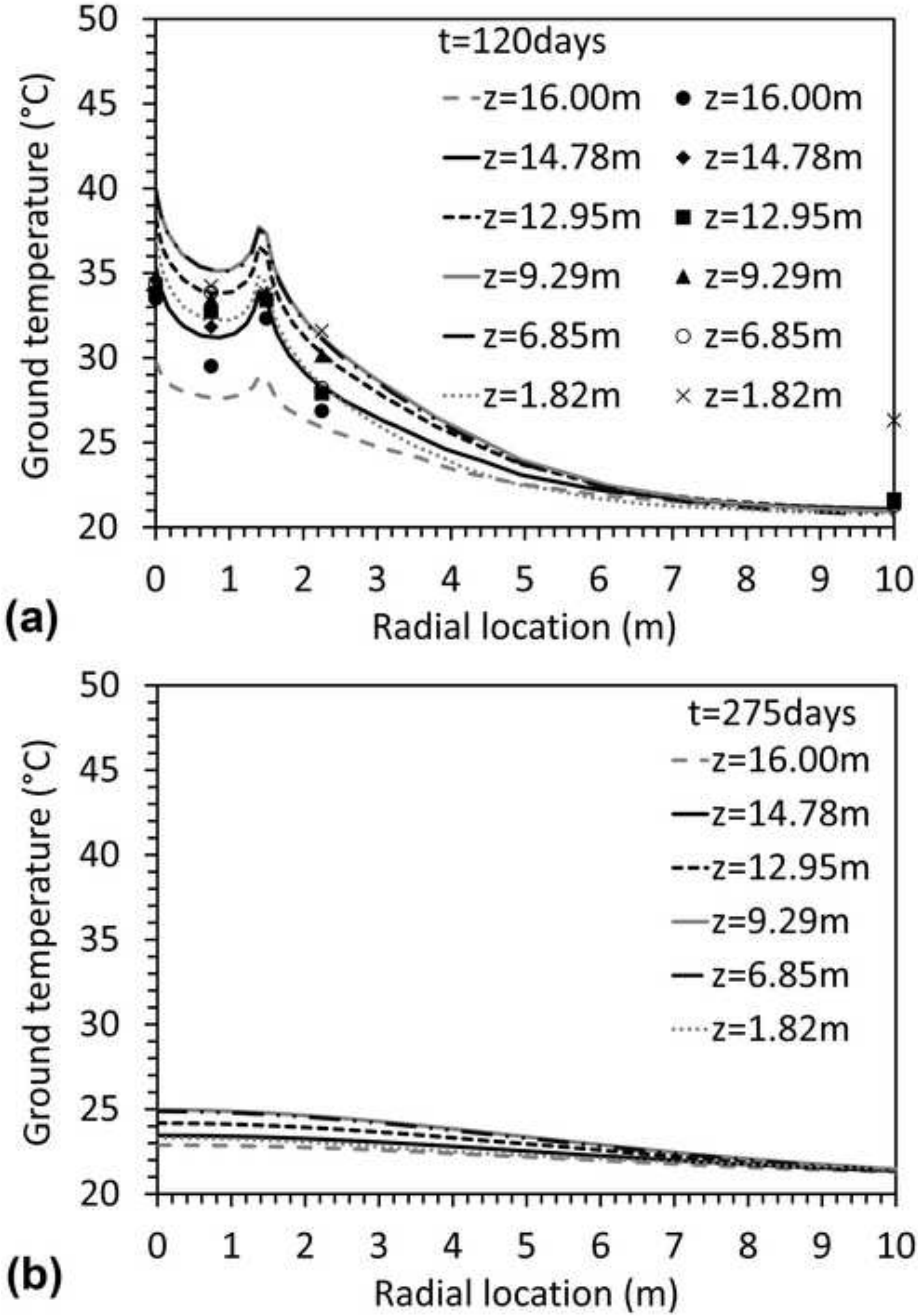

Figure 16
Click here to download high resolution image

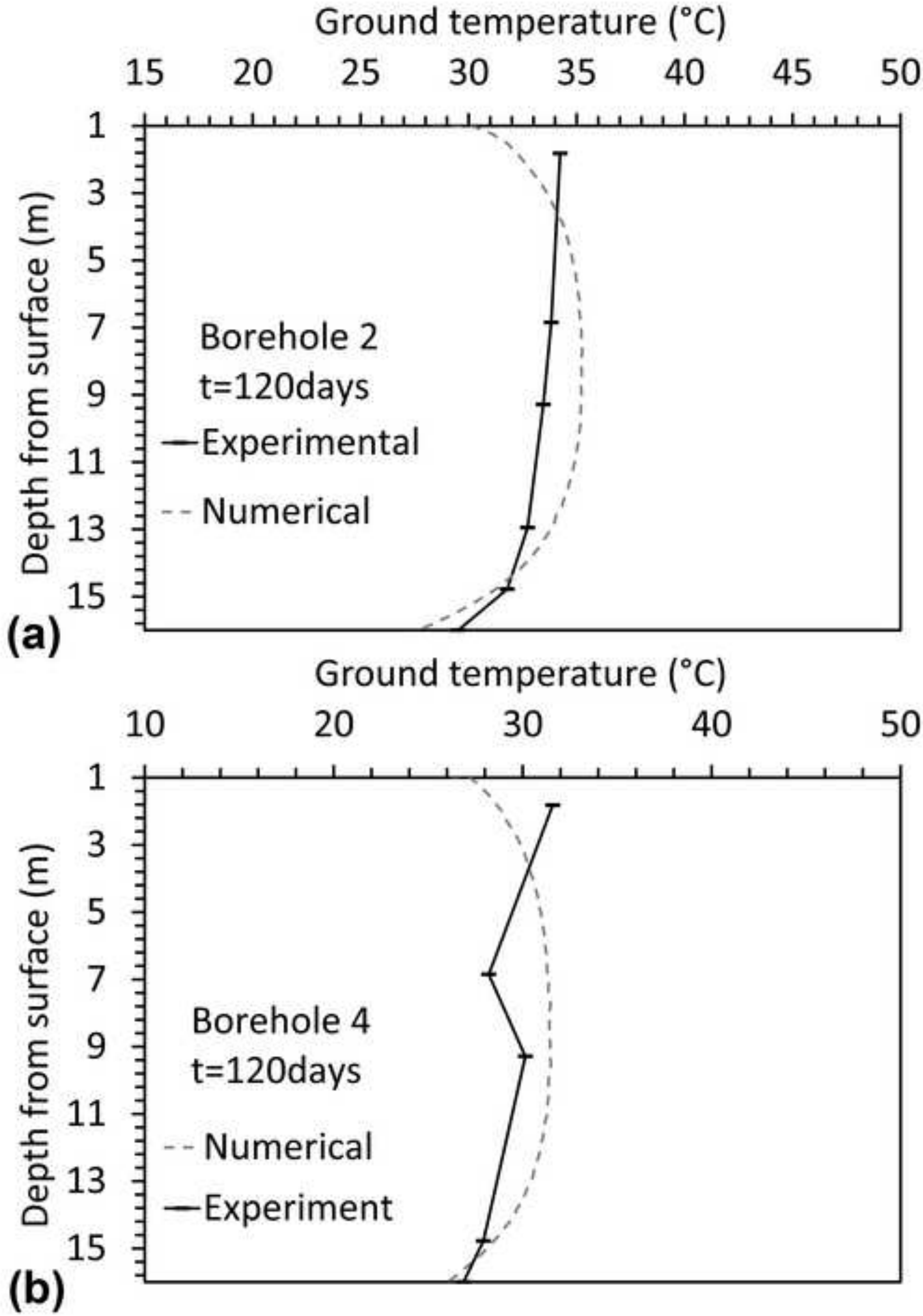

Figure 17
Click here to download high resolution image

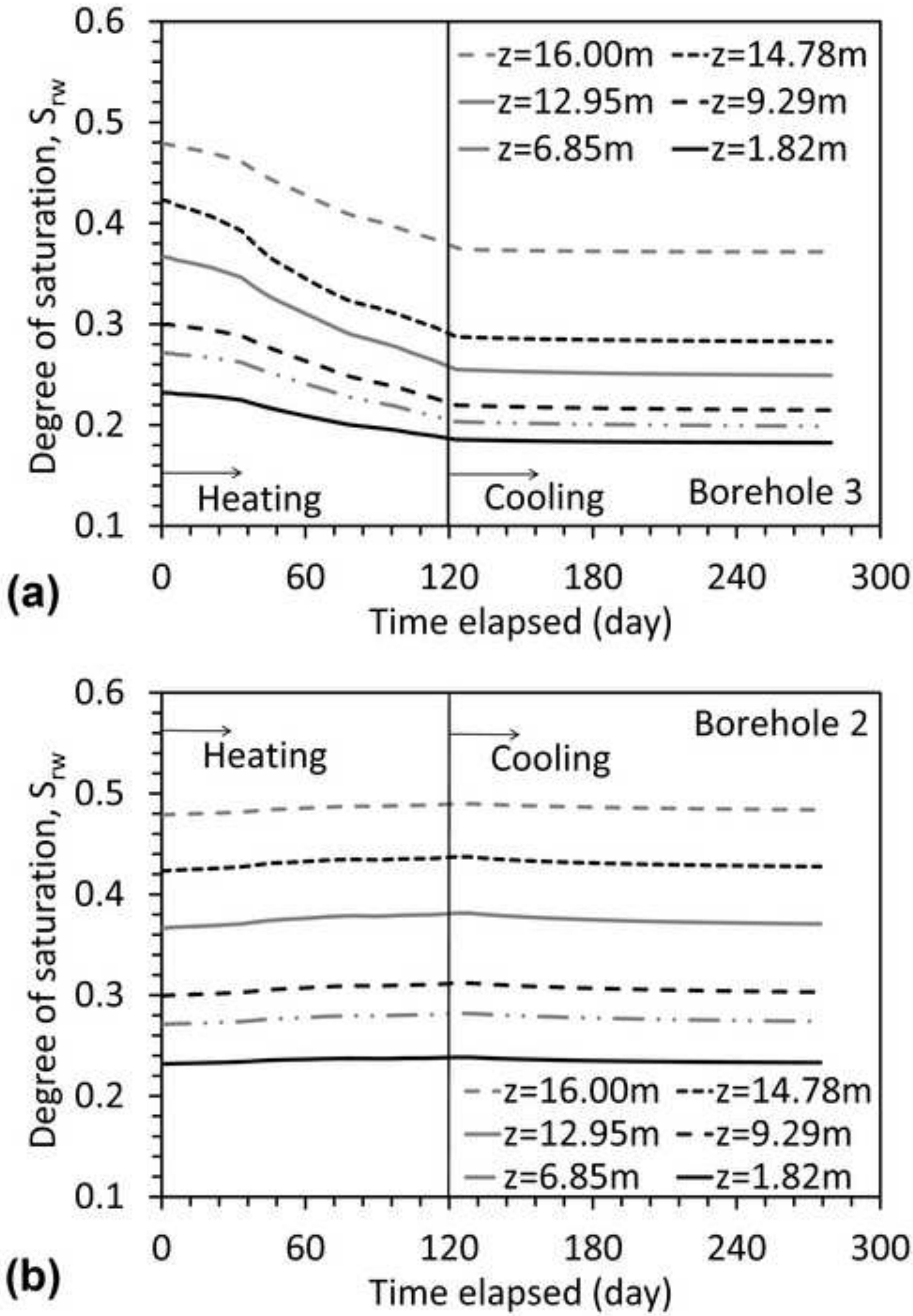

Figure 18
Click here to download high resolution image

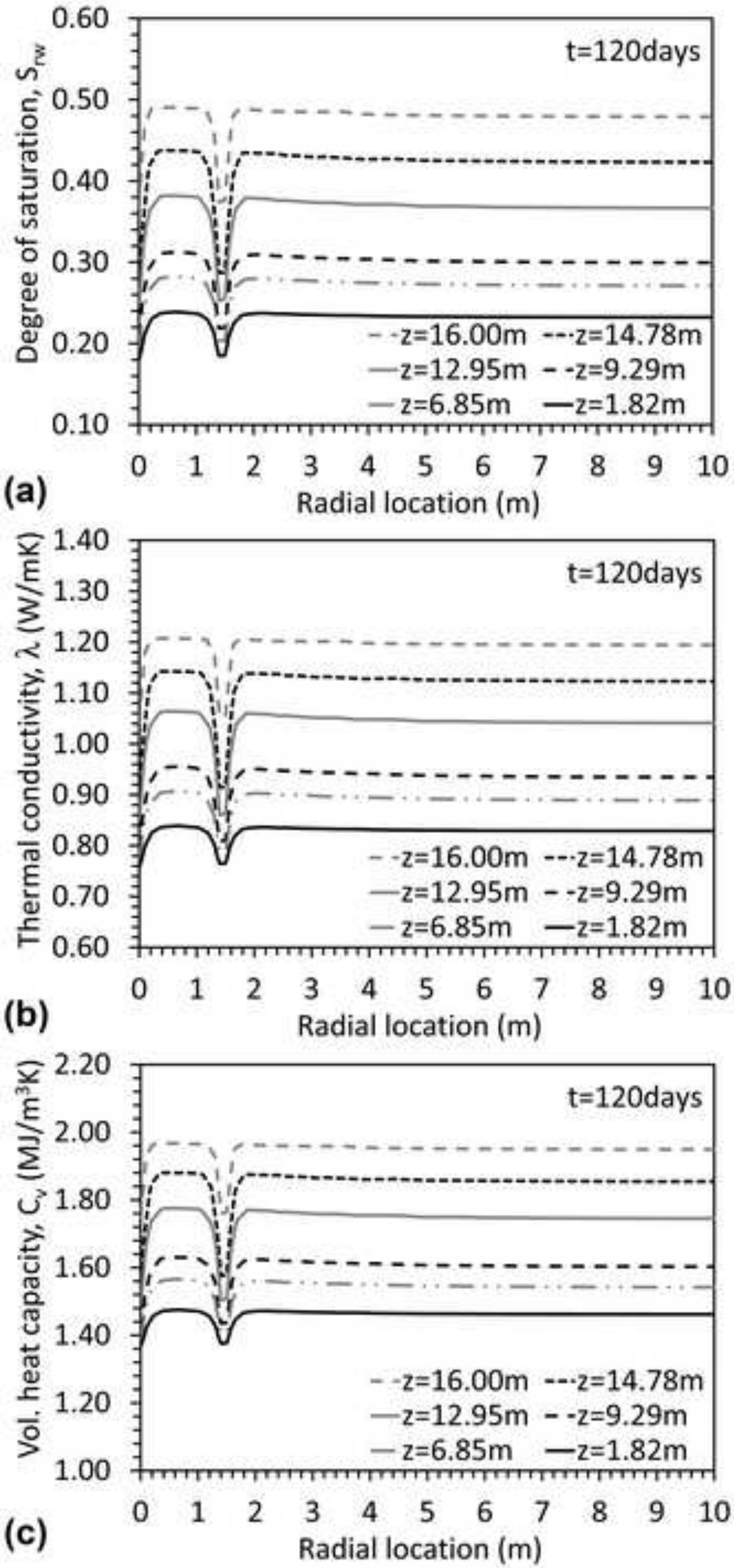

Figure 19
Click here to download high resolution image